Effective transport properties for periodic multiphase fiber-reinforced composites with complex constituents and parallelogram unit cells

F. J. Sabina[1,*], R. Guinovart-Díaz[2], Y. Espinosa-Almeyda[1], R. Rodríguez-Ramos[2,7], J. Bravo-Castillero[1,3], J. C. López-Realpozo[2], D. Guinovart-Sanjuán[4], T. Böhlke[5], J. Sánchez-Dehesa[6]

[1]Instituto de Investigaciones en Matemáticas Aplicadas y en Sistemas. Universidad Nacional Autónoma de México, Apartado Postal 20-126. Alcaldía Álvaro Obregón, 01000, CDMX, México

fjs@mym.iimas.unam.mx, yoanhealmeyda1209@gmail.com, julian@mym.iimas.unam.mx

[2]Facultad de Matemática y Computación. Universidad de La Habana, San Lázaro y L, Vedado, Habana 4, 10400, Cuba

guino@matcom.uh.cu, reinaldo@matcom.uh.cu, jclrealpozo@matcom.uh.cu

[3]Instituto de Investigaciones en Matemáticas Aplicadas y en Sistemas. Universidad Nacional Autónoma de México Mérida, Unidad Académica de Yucatán, Parque Científico Tecnológico de Yucatán, 97302, Mérida, México

[4]Department of Mathematics, University of Central Florida, 4393 Andromeda Loop N, Orlando, FL 32816, USA

davidgs1601@gmail.com,

[5]Chair for Continuum Mechanics, Institute of Engineering Mechanics, Karlsruhe Institute of Technology (KIT), Kaiserstr. 10, 76131 Karlsruhe, Germany.

thomas.boehlke@kit.edu

[6]Grupo de Fenómenos Ondulatorios, Departamento de Ingeniería Electrónica, Universitat Politécnica de València, Camino de Vera s.n. (Edificio 7F), Valencia, ES-46022, Spain.

jsdehesa@upv.es

[7]Escuela de Ingeniería y Ciencias, Tecnológico de Monterrey, Campus Puebla Atlixcáyotl 5718, Reserva Territorial Atlixcáyotl, 72453 Puebla, México.

*Corresponding author email: fjs@mym.iimas.unam.mx

Keywords: multi-phase fiber-reinforced composites; interface/interphase; asymptotic homogenization method; effective complex permittivity; transport problems

Abstract

The two-scale asymptotic homogenization method is used to find closed-form formulas for effective properties of periodic multi-phase fiber-reinforced composites where constituents have complex-valued transport properties and parallelogram unit cells. An antiplane problem relevant to linear elasticity is formulated in the frame of transport properties. The application of the method leads to the need of solving some local problems whose solution is found using potential theory and shear effective coefficients are explicitly obtained for $n-$phase fiber-reinforced composites. Simple formulae are explicitly given for three- and four-phase fiber-reinforced composites. The broad applicability, accuracy and generality of this model is determined through comparison with other methods reported in the literature in relation to shear elastic moduli and several transport problems of multi-phase fiber-reinforced composites in their realm, such as conductivity in a biological context and permittivity leading to gain and loss enhancement of dielectrics. Also, the example of gain enhancement of inertial mass density is looked into. Good agreement with other theoretical approaches is obtained. The formulas may be useful as benchmarks for checking experimental and numerical results.

1. Introduction

The prediction of effective transport properties of periodic composites, such as shear, electrical and thermal conductivities, permittivity, dielectric constant, magnetic permeability, thermal expansion, etc., is still important in applications (Giraud et al., 2019; Godin, 2013, 2016; Kaddouri et al., 2016; Kolpakov and Kolpakov, 2009; McCullough, 1985).

Multi-phase fiber-reinforced composites (FRC) have also received great attention by researches due to its wide field for transport problems. For example: Perrins et al. (1979) applied an extension of Rayleigh's method to calculate effective conductivity of FRC with a regular array of conductive cylindrical inclusions. The effective conductivity tensor is computed for a two-dimensional composite with doubly periodic array of circular inclusions (Godin, 2012). Real and imaginary parts of particulate homogenized composite material with complex-values constituent properties relative to permittivity are reported by (Mackay and Lakhtakia, 2016). The effective thermal conductivity of a transversely isotropic multi-phase FRC is predicted using the generalized self-consistent method (GSCM) and the energy balance principle (Hassan et al., 2013). The GSCM is previosly applied to analyze the interfacial contact conductance effect on effective thermal conductivity of particulate, transversely isotropic fiber and multi-layered composites (Lee et al., 2006). The mechanical deformation response of conductive FRC is studied as result of electric fields applications in the fibers's direction and considering electro-magneto-thermo-mechanical coupled effects (Perchikov and Aboudi, 2017).

Models have been developed for study heterogeneous multi-phase FRC. The main challenge of these is to establish, from the engineering point of view, a full process to optimize effective properties of FRC. Due to the complexity of the microstructure and the material properties, the digital twin composite must take into account the nature of two or even multiple scales, the constituents' specific geometrical and physical properties and characteristics of existent phases (Görthofer et al., 2019). For example: GSCM is implemented to compute effective transverse shear modulus of multi-interphase FRC (Dasgupta and Bhandarkar, 1992). The same scheme is applied to predict effective properties of homothetic particle-reinforced composite (Bonfoh et al., 2014). In that work, a general formulation for *n*-phase multi-coated composite with ellipsoidal inclusion is proposed. The upper and lower bounds of effective magnetic permeability of homogeneous and isotropic two-phase composite are derived by variational approach (Hashin and Shtrikman, 1962). Analytical expressions of effective coefficients are found by two-scale asymptotic homogenization method (AHM) for two-phase elastic fibrous composites with square (Rodríguez-Ramos et al., 2001) and hexagonal (Guinovart-Díaz et al., 2001) unit cells and transversely isotropic real-values constituents. A recursive scheme based on AHM is developed in order to find effective properties of multiphase unidirectional elastic FRC with transversely isotropic constituents and hexagonal symmetry (Guinovart-Díaz et al., 2005). The equivalent

inclusion concept (Eshelby, 1957) combining with the doubly quasi-periodic Riemann boundary value problem (Lu, 1994) is used to solve the problem of doubly periodic cylindrical inclusions under longitudinal shear (Jiang et al., 2004). A new micromechanical based on Green's functions technique and integral equation is developed to estimate effective elastic properties of multi-coated reinforce composite (Dinzart et al., 2016). The thermal conductivities of multiphase composites reinforced by carbon fibers is investigated by finite element method (Ahmadi et al., 2019). The effect of fiber hexagonal and random arrangements on elastic behavior of FRC is studied by finite element simulations (Beicha et al., 2016). The linear elastic properties are preddicted by mean field and full field approaches for short FRC (Müller et al., 2015). Here, the approaches are compared in detail, clearly indicating that the applicability of mean field approaches depends on the phase contrast in the phases. Mean field predictions are compared to experimental data in (Müller et al., 2016).

On the other hand, multi-phase models are also frequently used to simulate fiber-matrix adhesion regions in FRC. Here, a thin interphase illustrates a fiber–matrix transition zone, as a thin layer between them (so called imperfect contact region); see for instance (Hashin, 2001; Hashin, 2002; Sevostianov et al., 2012). Descriptions and analysis of imperfect interface conditions have been addressed by (Otero et al., 2013; Palla and Stefano, 2016), among others. Effects of non-uniform imperfect contact region between fiber and matrix on effective shear moduli are studied by (Guinovart-Díaz et al., 2013; 2016; López-Realpozo et al., 2014)

The main aim of this work is the effective transport complex properties prediction of periodic multi-phase FRC with complex-valued constituent properties and parallelogram cell by AHM. In addition, the effect of multiple interphases on quality of effective properties is also studied. As a particular case of transport complex properties, the analytical expression of antiplane local problems and effective shear properties are stated for a periodic $n-$phase FRC. Besides, the corresponding simple formulae for three- and four-phase FRC are given. Finally, due to the mathematical analogy and applicability of the present model in other transport problems, the determination of effective complex permittivity, conductivity of a biological tissue comprising by tubular cells, and enhanced permittivity with electromagnetic waves using lossy materials (in composites where the unidirectional inclusions are revisited by an annular interphase) are also analyzed as a multi-phase composite. Numerical analysis and validations of results are carried

out for two-, three- and four-phase FRC and discussed. Good agreements are obtained as benchmark for further experimental results.

The novelty of the present model is the extension to $n-$phase FRC with complex-valued constituent properties and periodic parallelogram-like cell using AHM. It generalizes previous results obtained by the same method for two-phase composites with periodic square (Rodríguez-Ramos et al., 2001), hexagonal (Guinovart-Díaz et al., 2001) and parallelogram (Guinovart-Díaz et al., 2011; Rodríguez-Ramos et al., 2011) cells and transversely isotropic real-values constituents.

2. General considerations

Let us consider a periodic *n*–phase FRC $\Pi \subset \mathbb{R}^3$ in the system of coordinates $\mathbf{x} = \{x_1, x_2, x_3\}$. The composite geometric description Π is defined by a parallelepiped-like array of $n-1$ concentric, unidirectional and infinitely longs cylinders embedded in matrix, without overlapping between them, as shown in Fig. 1(a). The material constituents of matrix and fibers phases (central fiber and $n-2$ coated fibers) are assumed elastic belonging to crystal symmetry class 6mm. The axes of material and geometric symmetry are parallel. In addition, as a unidirectional fibrous composite, it is considered that the microstructure remains constant along fiber x_3 direction (i.e., perpendicular to plane of cross-section) with complex-valued properties.

The composite's structure is characterized by periodicity of its microstructure, then, the composite's fiber cross-section (periodic unit cell Y) is a parallelogram (matrix) with $n-1$ concentric circles (fibers), see Fig. 1(b). The parallelogram-like unit cell Y is defined by a constant angle θ and the principal periods w_1 and w_2 over Oy_1y_2-plane in $\mathbf{y} = \{y_1, y_2, y_3\}$ system. Also, it is satisfied that $\mathrm{Y} = \bigcup_{i=1}^{n} S_i$ where S_1 is the region occupied by matrix limited by a parallelogram Σ with a circular hole of radius R_1, contour Γ_1 and volume V_1, S_r of volume V_r $(r = 2, \cdots, n-1)$ represents the region occupied by the ring (coated fibers) limited by circular interfaces Γ_{r-1} and Γ_r of radius R_{r-1} and R_r $(r = 2, \cdots, n-1)$, respectively, and S_n is occupied by central fiber limited by Γ_{n-1} with radius R_{n-1} and volume V_n. The thickness of the region

occupied by the $n-2$ coated fibers is $\boldsymbol{h}$ and r-th interphase thickness is $h_r = R_{r-1} - R_r$ (see Fig.2). The circular interface Γ_s $(s = 1, \cdots, n-1)$ is defined as $\Gamma_s = \left\{ \mathrm{z} = R_s e^{i\theta}, 0 \le \theta \le 2\pi \right\}$ and the volume V of Y satisfies that $\mathrm{V} = \mathrm{V}_1 + \sum_{r=2}^{n-1} \mathrm{V}_r + \mathrm{V}_n = 1$. The macro and micro-scale relation $\mathbf{y} = \mathbf{x} / \varepsilon$ is measured from a small geometrical parameter $\varepsilon = l / \mathrm{L}$, which relates the distance (l) between the centers of two neighboring cylinders and the diameter (L) of the composite.

Fig. 1

Fig. 2

In the forthcoming sections some summary ideas of the antiplane problems and a brief comment about AHM are given. The antiplane local problems statement and its corresponding solutions are shown. The effective coefficients for multi-phase FRC are calculated analytically and numerically in order to obtain effective transport complex-values properties. Analysis of results is discussed.

3. Two-scale asymptotic homogenization method (AHM) applied to elasticity problem for a multi-phase fiber reinforced composite. Antiplane problems $_{\alpha 3}\mathrm{L}$

In material science, the estimation of effective transport properties of periodic composites is a field of interest associated to practical situations. Transport problems (for example: problems of heat conduction, diffusion, electrostatic, magnetostatic, elasticity theory, among others) is represented by an equilibrium linear equation

$$\operatorname{div} \mathbf{F} = \mathbf{f}(x), \tag{1}$$

with the constitutive relation

$$\mathrm{F}_i = K_{ij} \frac{\partial \Phi}{\partial x_i}, \tag{2}$$

where $i,\ j = 1, 2, 3$. Herein, F_i is the component of an induced flux **F** (heat flux, diffusion current density, electric displacement, magnetic induction, stress and so on), Φ represents a harmonic

potential (temperature, density, electric and magnetic potentials, displacement, etc.) and $\partial\Phi/\partial x_i$ their gradient (temperature and density gradients, electric and magnetic fields, strain and others). K_{ij} are components of linear responses tensor (or transport properties) of an analyzed medium, i.e., thermal conductivity, diffusivity, dielectric and magnetic permittivity, stiffness moduli, and the like. $\mathbf{f}(x)$ represents the body force vector. Many works focused on characterization of composite's transport properties with different physical and structural conditions are reported by (Kolpakov and Kolpakov, 2009; Pal, 2014; Yan et al., 2018), and its references.

In this work, a particular transport problem in linear elasticity is considered. Herein, an antiplane mechanical deformation state problem for a multi-phase FRC is solved. Hence, the corresponding constitutive equations (Eq. (2)) for a heterogeneous structures are given by components as (Nemat-Nasser and Hori, 1993):

$$\sigma_{\beta 3} = \mathrm{C}_{\beta 3 \beta 3} u_{3,\beta}, \tag{3}$$

with $\beta = 1, 2$. In this, the induced flux $\mathrm{F}_i \left(\equiv \sigma_{\beta 3}\right)$ represents antiplane mechanical stress, the linear response tensor $K_{ij} \left(\equiv \mathrm{C}_{\beta 3 \beta 3}\right)$ denotes elastic modulus, and $\Phi\left(\equiv u_3\right)$ is the only non-null mechanical displacement. The comma denotes partial differentiation relative to x_β component.

Consequently, for a static case and in absences of body forces, the following classical elliptic boundary value problem with Y-periodic and rapidly oscillating coefficients is necessary to solve:

$$\left(\mathrm{C}_{3\eta 3\beta}(\mathbf{y}) u_{3,\beta}\right)_{,\eta} = 0, \quad \text{in } \Pi, \tag{4}$$

subject to perfect conditions at Γ_s together with boundary conditions on $\partial\Pi$

$$[[\mathrm{C}_{1313} u_{3,\beta}\, n_\beta]]\big|_{\Gamma_s} = 0, \quad [[u_3]]\big|_{\Gamma_s} = 0, \tag{5}$$

$$(\sigma_{3j} n_j)\big|_{\partial\Pi} = \mathrm{T}_0, \quad u_3\big|_{\partial\Pi} = u_0, \tag{6}$$

where $\beta, \eta = 1, 2$. In Eqs. (5) and (6), u_0 (displacement) and T_0 (traction) are infinitely differentiable functions on the external boundary of Π. The double square brackets notation $[[f]]\big|_{\Gamma_s} = f^{(s)} - f^{(s+1)}$ $(s = 1, \cdots, n-1)$ represents the jump of f across the circular interface Γ_s and $\mathbf{n} = (n_1, n_2)$ is the unit normal vector to Γ_s. The usual convention index sum is considered.

The asymptotic solution of elliptic boundary value problem (Eqs. (4)-(6)) is found by representing u_3 as an asymptotic series in powers of small parameter ε by the ansatz:

$$u_3(\mathbf{x}) = v_0(\mathbf{x}) + \varepsilon v_1(\mathbf{x},\mathbf{y}) + O(\varepsilon^2), \tag{7}$$

where $v_0(\mathbf{x})$ is independent of $\mathbf{y}$ and $v_1(\mathbf{x},\mathbf{y})$ is a Y-periodic function respect to local variable $\mathbf{y}$. In addition, it is satisfied that $v_1(\mathbf{x},\mathbf{y}) = {}_{\alpha 3}N(\mathbf{y})v_{0,\alpha}(\mathbf{x})$ where ${}_{\alpha 3}N(\mathbf{y})$ is a Y-periodic local function independent of the global variable **x**.

Following the methodology developed in the works (Bakhvalov and Panasenko, 1989; Pobedrya, 1984) the well-known AHM is applied here. Therefore, the determination of the antiplane local problems and the associated effective moduli of multi-phase FRC over Y is the main aim of this section. Likewise, we consider a heterogeneous material occupying the region Y and the properties takes different values in each component of the composite.

Thus, if Eq. (7) is substituted into Eqs. (4)-(6) taking into account the change of scale relate to **x** and **y**, and subsequently, the resulting expressions are grouped according to power of ε, the formulation of antiplane local problems on Y and equivalent homogenized problem, as well as, the antiplane effective coefficients formulae are obtained.

Hence, the mathematical statement of antiplane local problems on Y, denoted as ${}_{\alpha 3}L$ $(\alpha = 1,2)$, for a $n-$phase FRC can be stated by:

The Laplace equations,

$$\left(C_{1313} + C_{1313\,\alpha 3}N_{,\beta}\right),_{\beta} = 0 \qquad \text{in } S_{\gamma} \ (\gamma = 1,\cdots,n), \tag{8}$$

with perfect contact condition at interfaces Γ_s $(s = 1,\cdots,n-1)$:

$${}_{\alpha 3}N^{(s)}\big|_{\Gamma_s} = {}_{\alpha 3}N^{(s+1)}\big|_{\Gamma_s}, \tag{9}$$

$$\left[\left(C^{(s)}_{1313\,\alpha 3}N^{(s)}_{,\beta} - C^{(s+1)}_{1313\ \alpha 3}N^{(s+1)}_{,\beta}\right)n_{\beta}\right]\Big|_{\Gamma_s} = -\left[\left(C^{(s)}_{1313} - C^{(s+1)}_{1313}\right)\left(\delta_{1\alpha}\, n_1 + \delta_{2\alpha}\, n_2\right)\right]\Big|_{\Gamma_s}, \tag{10}$$

and the condition

$$\left\langle {}_{\alpha 3}N^{(s)} \right\rangle = 0, \quad \text{in Y}. \tag{11}$$

Here, ${}_{\alpha 3}N \equiv {}_{\alpha 3}N(\mathbf{y})$ is an unknown Y−periodic harmonic local function which it is solution of the ${}_{\alpha 3}L$ problems. The operator $\langle f \rangle$ is the volume average of f per unit length over the unit

cell Y, i.e., $\langle f \rangle = \mathrm{V}^{-1}\int_{\mathrm{Y}} f(\mathrm{y})\,\mathrm{dy}$. ${}_{\alpha 3}\mathrm{N}^{(s)}_{,\beta}$ is the derivative of ${}_{\alpha 3}\mathrm{N}^{(s)}$ with respect to the local variable y_β, and $\delta_{1\alpha}(\delta_{2\alpha})$ is Kronecker's delta function related to the local problem ${}_{13}\mathrm{L}({}_{23}\mathrm{L})$.

Consequently, the equivalent homogenized problem is stated, as follows:

$$\mathrm{C}^{*}_{3\alpha 3\beta}\mathrm{v}_{0,\alpha\beta}(\mathbf{x}) = 0\,,\ (\alpha = 1,2) \tag{12}$$

subject the boundary conditions $\mathrm{v}_0(\mathbf{x}) = \mathrm{T}^0(\mathbf{x})$ on $\partial\Pi$.

In Eq. (12), $\mathrm{C}^{*}_{3\alpha 3\beta}$ represents the antiplane effective coefficients and they are defined as follows:

$$\mathrm{C}^{*}_{3\alpha 3\beta} = \left\langle \mathrm{C}_{3\alpha 3\beta}(\mathbf{y}) + \mathrm{C}_{3\alpha 3\eta}(\mathbf{y})\,{}_{\alpha 3}\mathrm{N}_{,\eta}(\mathbf{y}) \right\rangle, \tag{13}$$

also, $\mathrm{v}_0(\mathbf{x})$ is solution of the homogenized equation and $\mathrm{T}^0(\mathbf{x})$ is an infinitely differential function.

Now, in order to find the antiplane effective coefficients, the unknown local functions ${}_{\alpha 3}\mathrm{N}$ need to be found. Therefore, the analytical solution of Eqs. (8)-(11) is calculated.

4. Solution of the antiplane local problems ${}_{\alpha 3}\mathrm{L}$ for a multi-phase fiber-reinforced composite

Considering the mathematical statement of the antiplane local problems (Eqs. (8)-(11)), the unknown doubly periodic harmonic local functions ${}_{\alpha 3}\mathrm{N}^{(s)}$ are determined by means of Laurent expansion of harmonic functions over the matrix region S_1, such as,

$${}_{\alpha 3}\mathrm{N}^{(1)} = \mathrm{Re}\left\{ {}_{\alpha 3}a_0\, z\, R_1^{-1} + \sum_{p=1}^{\infty}{}^{o}\sum_{k=1}^{\infty}{}^{o}\,{}_{\alpha 3}a_k \eta_{kp} R_1^{-p} z^p + \sum_{p=1}^{\infty}{}^{o}\,{}_{\alpha 3}a_p\, R_1^p z^{-p} \right\}, \tag{14}$$

by the sum of power expansions in S_r

$${}_{\alpha 3}\mathrm{N}^{(r)} = \mathrm{Re}\left\{ \sum_{p=1}^{\infty}{}^{o}\,{}_{\alpha 3}b_p^{(r)} R_r^{-p} z^p + \sum_{p=1}^{\infty}{}^{o}\,{}_{\alpha 3}b_{-p}^{(r)}\, R_{r-1}^{p} z^{-p} \right\}, \tag{15}$$

and power expansions in S_n

$${}_{\alpha 3}\mathrm{N}^{(n)} = \mathrm{Re}\left\{ \sum_{p=1}^{\infty}{}^{o}\,{}_{\alpha 3}c_p\, R_{n-1}^{-p} z^p \right\}, \tag{16}$$

where, the undetermined coefficients ${}_{\alpha 3}a_0$, ${}_{\alpha 3}a_p$, ${}_{\alpha 3}a_k$, ${}_{\alpha 3}b_p^{(r)}$, ${}_{\alpha 3}b_{-p}^{(r)}$ $(r = 2,\cdots,n-1)$ and ${}_{\alpha 3}c_p$

are complex and they depend on the solution of the antiplane local problem ${}_{\alpha 3}\mathrm{L}$ to be solved. From Eqs. (14)-(16), it can be emphasized that the summation symbol with superscript $\sum_{p=1}^{\infty}{}^{o}$ means that the sum only runs over odd integers, the symbols Re (Im) is the real (imaginary) part of the complex number and $z = y_1 + iy_2$ is a complex variable on the cell Y. In addition, $\eta_{kp} = -\dfrac{(k+p-1)!}{p!(k-1)!} R^{k+p} \sum_{m,n}^{\infty} \beta_{mn}^{-(k+p)}$, such as $\beta_{mn} = mw_1 + nw_2$, $m^2 + n^2 \neq 0$, $k + p > 2$.

From the double periodicity condition of ${}_{\alpha 3}\mathrm{N}$ the following relations are satisfied

$$ {}_{\alpha 3}\mathrm{N}(z + w_\alpha) - {}_{\alpha 3}\mathrm{N}(z) = \mathrm{Re}\left\{ {}_{\alpha 3}a_0 R_1^{-1} w_\alpha + {}_{\alpha 3}a_1 \delta_\alpha R_1 \right\}, \tag{17} $$

here, $\delta_\alpha = \zeta(z + w_\alpha) - \zeta(z) = 2\zeta(w_\alpha / 2)$ is the quasi-periodic condition and $\zeta(z)$ is the Weierstrass quasi-periodic Zeta function of periods w_1 and w_2, such that $\zeta(z) = z^{-1} + \sum{}'_{m,n}\left[\left(z - \beta_{mn}\right)^{-1} + \beta_{mn}^{-1} + z\beta_{mn}^{-2} \right]$, see (Grigolyuk and Fil'shtinskii, 1970). The summation symbol with the prime superscript $\sum{}'_{m,n}$ means that the summation does not include the point $(m, n) = (0, 0)$. Thus, it can be concluded that ${}_{\alpha 3}a_0 = -R_1^2 H_1 \, {}_{\alpha 3}\overline{a}_1 - R_1^2 H_2 \, {}_{\alpha 3}a_1$ with $H_1 = \left(\overline{\delta}_1 \overline{w}_2 - \overline{\delta}_2 \overline{w}_1\right) / \left(w_1 \overline{w}_2 - w_2 \overline{w}_1\right)$ and $H_2 = \left(\delta_1 \overline{w}_2 - \delta_2 \overline{w}_1\right) / \left(w_1 \overline{w}_2 - w_2 \overline{w}_1\right)$.

Finally, if the expansions Eqs. (14)-(16) are replaced into Eqs. (9) and (10), and some algebraic calculations are developed, the next system is found in order to compute the complex undetermined coefficients ${}_{\alpha 3}a_k$, ${}_{\alpha 3}\overline{a}_p$, ${}_{\alpha 3}b_p^{(s_1)}$, ${}_{\alpha 3}\overline{b}_{-p}^{(s_1)}$ $(s_1 = 2, \cdots, n-2)$ and ${}_{\alpha 3}c_p$ that is:

$$
\begin{aligned}
{}_{\alpha 3}a_0 \delta_{1p} + \sum_{k=1}^{\infty}{}^{*} {}_{\alpha 3}a_k \eta_{kp} + {}_{\alpha 3}\overline{a}_p - {}_{\alpha 3}b_p^{(2)} R_1^p R_2^{-p} - {}_{\alpha 3}\overline{b}_{-p}^{(2)} &= 0, \\
{}_{\alpha 3}b_p^{(s_1)} + {}_{\alpha 3}\overline{b}_{-p}^{(s_1)} R_{s_1-1}^p R_{s_1}^{-p} - {}_{\alpha 3}b_p^{(s_1+1)} R_{s_1}^p R_{s_1+1}^{-p} - {}_{\alpha 3}\overline{b}_{-p}^{(s_1+1)} &= 0, \\
{}_{\alpha 3}b_p^{(n-1)} + {}_{\alpha 3}\overline{b}_{-p}^{(n-1)} R_{n-2}^p \, R_{n-1}^{-p} &= {}_{\alpha 3}c_p, \\
{}_{\alpha 3}a_0 \delta_{1p} + \sum_{k=1}^{\infty}{}^{*} {}_{\alpha 3}a_k \eta_{kp} - {}_{\alpha 3}\overline{a}_p - k_1 \, {}_{\alpha 3}b_p^{(2)} R_1^p R_2^{-p} + k_1 \, {}_{\alpha 3}\overline{b}_{-p}^{(2)} &= (k_1 - 1) R_1 \delta_{1p} \left[\delta_{1\alpha} - i\delta_{2\alpha}\right], \\
k_{s_1-1}\left[{}_{\alpha 3}b_p^{(s_1)} - {}_{\alpha 3}\overline{b}_{-p}^{(s_1)} R_{s_1-1}^p R_{s_1}^{-p} \right] - k_{s_1}\left[{}_{\alpha 3}b_p^{(s_1+1)} R_{s_1}^p R_{s_1+1}^{-p} - {}_{\alpha 3}\overline{b}_{-p}^{(s_1+1)} \right] &= \left(k_{s_1} - k_{s_1-1}\right) R_{s_1} \delta_{1p} \left[\delta_{1\alpha} - i\delta_{2\alpha}\right], \\
k_{n-2}\left[{}_{\alpha 3}b_p^{(n-1)} - {}_{\alpha 3}\overline{b}_{-p}^{(n-1)} R_{n-2}^p R_{n-1}^{-p} \right] - k_{n-1} \, {}_{\alpha 3}c_p &= \left(k_{n-1} - k_{n-2}\right) R_{n-1} \delta_{1p} \left[\delta_{1\alpha} - i\delta_{2\alpha}\right].
\end{aligned}
\tag{18}
$$

In Eq. (18), δ_{1p} is the Kronecker's delta function, $k_s = C_{1313}^{(s+1)} / C_{1313}^{(1)}$ $(s = 1, \cdots, n-1)$ and the

overbar is the complex conjugate. As can be seen, the system Eq. (18) is a normal infinity system of $2n-2$ linear equations, see for instance (Kantorovich and Krylov, 1964). Due to its size and complexity, it can be solve by means of truncation orders (N_0) to generate approximations through $2n-2$ blocks with $2n-2$ unknown complex coefficients (for $k, p = 1,3,5,\cdots$). Then, new blocks (sub-matrix systems) are solved by Gauss's method. A rapidly convergence of successive truncations is guaranteed due to the system regularity (Rodríguez-Ramos et al., 2012), so that successive approximations are used. Also, the system solutions of each local problem ${}_{\alpha 3}\mathrm{L}$ depend on the elastic material constituents, phase volumes and the spatial distributions of fibers in matrix related to the problem. Once we have the unknown coefficients ${}_{\alpha 3}a_k$, ${}_{\alpha 3}\overline{a}_p$, ${}_{\alpha 3}b_p^{(s_1)}$, ${}_{\alpha 3}b_{-p}^{(s_1)}$ and ${}_{\alpha 3}c_p$, the effective coefficients are computed as below.

The analytical formulae of the antiplane effective coefficients (Eq. (13)) for multi-phase FRC associated with the antiplane local problems ${}_{\alpha 3}\mathrm{L}$ are also shown. They are obtained by means of the Green's theorem for multiple connected regions to the area integrals in plane Oy_1y_2, and subsequently, replacing expansions Eq., (14)-(16) into the integrals and taking into account the double periodicity of the local functions and orthogonally properties of complex functions $\left\{e^{in\theta}\right\}_{-\infty}^{\infty} \equiv \left\{\cos n\theta, sin\, n\theta\right\}_{-\infty}^{\infty}$, see (Guinovart-Díaz et al., 2016; López-Realpozo et al., 2014). They are summarized as follows:

$$\mathrm{C}^*_{1313} - i\mathrm{C}^*_{2313} = \left\langle \mathrm{C}_{1313} \right\rangle - [[\mathrm{C}_{1313}]]_2 \frac{R_1\pi}{\mathrm{V}}\, {}_{13}A - \sum_{i=3}^{n-1} [[\mathrm{C}_{1313}]]_i \frac{R_{i-1}\pi}{\mathrm{V}}\, {}_{13}B^{(i-1)} - [[\mathrm{C}_{1313}]]_n \frac{R_{n-1}\pi}{\mathrm{V}}\, {}_{13}c_1, \quad (19)$$

$$\mathrm{C}^*_{1323} - i\mathrm{C}^*_{2323} = -i\left\langle \mathrm{C}_{1313} \right\rangle - [[\mathrm{C}_{1313}]]_2 \frac{R_1\pi}{\mathrm{V}}\, {}_{23}A - \sum_{i=3}^{n-1} [[\mathrm{C}_{1313}]]_i \frac{R_{i-1}\pi}{\mathrm{V}}\, {}_{23}B^{(i-1)} - [[\mathrm{C}_{1313}]]_n \frac{R_{n-1}\pi}{\mathrm{V}}\, {}_{23}c_1, \quad (20)$$

where ${}_{\alpha 3}A = \left[{}_{\alpha 3}a_0 + \sum_{k=1}^{\infty}{}^{*}\, {}_{\alpha 3}a_k \eta_{k1} + {}_{\alpha 3}\overline{a}_1 \right]$, ${}_{\alpha 3}B^{(i-1)} = \left[{}_{\alpha 3}b_1^{(i-1)} + {}_{\alpha 3}\overline{b}_{-1}^{(i-1)} R_{i-2}/R_{i-1} \right]$ and the symbol $[[C_{1313}]]_{s+1} = C_{1313}^{(s)} - C_{1313}^{(s+1)}$. As can be noted, effective properties are functions of the constituent properties, the fraction volumes of each phase, and the fundamental periods of Y by means of the system solutions associated to the antiplane local problem ${}_{13}\mathrm{L}$ or ${}_{23}\mathrm{L}$. The cell volume is $\mathrm{V} = |w_1||w_2|\, sen\theta$, $\left\langle \mathrm{C}_{1313} \right\rangle = \sum_{i=1}^{n} \mathrm{C}_{1313}^{(i)} \mathrm{V}_i$ is the Voigt average and $\sum_{i=1}^{n} \mathrm{V}_i = 1$.

4.1 Solution of the antiplane local problems ${}_{\alpha 3}\mathrm{L}$ and effective properties for a four-phase FRC.

In this section, the solution of the antiplane local problems and the analytical formulae of the antiplane effective coefficients for a periodic four-phase FRC (see Fig 2) are shown.
In this sense, the equivalent system of Eq. (18) is given as

$$\begin{aligned}
&{}_{\alpha 3}a_0\delta_{1p}+\sum_{k=1}^{\infty}{}^{*}\,{}_{\alpha 3}a_k\eta_{kp}+{}_{\alpha 3}\bar{a}_p-{}_{\alpha 3}b_p^{(2)}R_1^pR_2^{-p}-{}_{\alpha 3}\bar{b}_{-p}^{(2)}=0,\\
&{}_{\alpha 3}b_p^{(2)}+{}_{\alpha 3}\bar{b}_{-p}^{(2)}R_1^pR_2^{-p}-{}_{\alpha 3}b_p^{(3)}R_2^pR_3^{-p}-{}_{\alpha 3}\bar{b}_{-p}^{(3)}=0,\\
&{}_{\alpha 3}b_p^{(3)}+{}_{\alpha 3}\bar{b}_{-p}^{(3)}R_2^p\,R_3^{-p}={}_{\alpha 3}c_p,\\
&{}_{\alpha 3}a_0\delta_{1p}+\sum_{k=1}^{\infty}{}^{*}\,{}_{\alpha 3}a_k\eta_{kp}-{}_{\alpha 3}\bar{a}_p-k_1\,{}_{\alpha 3}b_p^{(2)}R_1^pR_2^{-p}+k_1\,{}_{\alpha 3}\bar{b}_{-p}^{(2)}=(k_1-1)R_1\delta_{1p}\left[\delta_{1\alpha}-i\delta_{2\alpha}\right],\\
&k_1\,{}_{\alpha 3}b_p^{(2)}-k_1\,{}_{\alpha 3}\bar{b}_{-p}^{(2)}R_1^pR_2^{-p}-k_2\,{}_{\alpha 3}b_p^{(3)}R_2^pR_3^{-p}+k_2\,{}_{\alpha 3}\bar{b}_{-p}^{(3)}=\left(k_2-k_1\right)R_2\delta_{1p}\left[\delta_{1\alpha}-i\delta_{2\alpha}\right],\\
&k_2\left[{}_{\alpha 3}b_p^{(3)}-{}_{\alpha 3}\bar{b}_{-p}^{(3)}R_2^pR_3^{-p}\right]-k_3\,{}_{\alpha 3}c_p=\left(k_3-k_2\right)R_3\delta_{1p}\left[\delta_{1\alpha}-i\delta_{2\alpha}\right].
\end{aligned}\tag{21}$$

The reduced normal linear system (Eq. (21)) can be represent in matrix form by 6×6 blocks for different k and p with unknown coefficients ${}_{\alpha 3}a_k$, ${}_{\alpha 3}\bar{a}_p$, ${}_{\alpha 3}b_p^{(2)}$, ${}_{\alpha 3}b_{-p}^{(2)}$, ${}_{\alpha 3}b_p^{(3)}$, ${}_{\alpha 3}b_{-p}^{(3)}$, and ${}_{\alpha 3}c_p$. Then, from the relation ${}_{\alpha 3}a_0=-R_1^2H_2\,{}_{\alpha 3}a_1-R_1^2H_1\,{}_{\alpha 3}\bar{a}_1$ and after some recurrent algebraic calculations, Eq. (21) can be re-written as follows

$${}_{\alpha 3}\bar{a}_p+\chi_1R_1^2H_1\delta_{1p}\,{}_{\alpha 3}\bar{a}_1+\chi_1R_1^2H_2\delta_{1p}\,{}_{\alpha 3}a_1-\chi_p\sum_{k=1}^{\infty}{}^{*}\,{}_{\alpha 3}a_kW_{kp}=ER_1\delta_{1p}\left[\delta_{1\alpha}-i\delta_{2\alpha}\right],\tag{22}$$

where $W_{kp}=\sqrt{pk^{-1}}\,\eta_{kp}$ and the expressions χ_p and E are summarized in Appendix A. It can be proved that ${}_{\alpha 3}b_p^{(2)}$, ${}_{\alpha 3}b_{-p}^{(2)}$, ${}_{\alpha 3}b_p^{(3)}$, ${}_{\alpha 3}b_{-p}^{(3)}$, and ${}_{\alpha 3}c_p$ depend on the coefficients ${}_{\alpha 3}a_k$ and ${}_{\alpha 3}\bar{a}_p$.
The solution of Eq. (22), analogous to (López-Realpozo et al., 2011) is found through two separate subsystems of real and imaginary magnitudes. Theses subsystems are obtained by replacing the complex variables ${}_{\alpha 3}a_k={}_{\alpha 3}x_k+i\,{}_{\alpha 3}y_k$, $W_{kp}=w_{1kp}+iw_{2kp}$ and $H_\alpha=h_{1\alpha}+ih_{2\alpha}$ into Eq. (22), with ${}_{\alpha 3}x_k$, ${}_{\alpha 3}y_k$, w_{1kp}, w_{2kp}, $h_{1\alpha}$ and $h_{2\alpha}$ real numbers and $i^2=-1$. Consequently, Eq. (21) can be rewritten in the matrix form as follows

$$\left(I+\chi_1R_1^2J\delta_{1p}+W\right)X=R_1E\delta_{1p}B,\tag{23}$$

where I is unit matrix and $J=\begin{pmatrix} h_{11}+h_{12} & h_{21}-h_{22} \\ -h_{21}-h_{22} & h_{11}-h_{12} \end{pmatrix}$. The square matrix $W\equiv W(w_{kp})$ is made up of different 2×2 blocks $w_{kp}=\chi_p\begin{pmatrix} w_{1kp} & -w_{2kp} \\ -w_{2kp} & -w_{1kp} \end{pmatrix}$ where *k* and *p* are odd natural numbers. The transposes of the infinite vectors X and B are $X^{\mathrm{T}}=(x_1,y_1,x_3,y_3,....)$ and $B^{\mathrm{T}}=(\delta_{1\alpha},\delta_{2\alpha})$ respectively.

In particular, if $k=p=1$ is considered, the system (Eq. (23)) can be reduced to a simple and compact form (so call short formulae), as follows

$$\left(I+\chi_1 R_1^2 J\right)X=R_1 EB\,, \tag{24}$$

where I is a unit matrix of order 2 and $X^{\mathrm{T}}=\begin{pmatrix} x_1 & y_1 \end{pmatrix}$. Here, x_k and y_k for $k\geq 3$ are null and $W\equiv 0$. This first approximation is equivalent to truncate the system, Eq. (23), to an order N_0 equal 1, and its solutions is easy to find,

$$X=R_1 E\left(I+\chi_1 R_1^2 J\right)^{-1}B\,. \tag{25}$$

For a higher truncation order (general case), the system (Eq. (23)) can be solved exactly by separating of $p=1$ and $p\geq 3$, and varying $k=1,3,\cdots$.

Thus, a closer look at the system (Eq. (23)) for $p=1$ gives

$$\left(I+\chi_1 R_1^2 J\right)X+N_1 X_1=R_1 EB\,, \tag{26}$$

where $X^{\mathrm{T}}=\begin{pmatrix} x_1 & y_1 \end{pmatrix}$, $N_1\equiv N_1(w_{k1})$ is an infinite matrix of 2×2 square blocks by rows with $N_1(w_{k1})=\chi_1\begin{pmatrix} w_{1k1} & -w_{2k1} \\ -w_{2k1} & -w_{1k1} \end{pmatrix}$, $k=2t+1$ and $X_1^{\mathrm{T}}\equiv(x_3,y_3,...,x_{2t+1},y_{2t+1},...)$.

Then, for $p\geq 3$ is computed that,

$$(I+W)X_1=-N_2X\,, \tag{27}$$

where $N_2\equiv N_2(w_{1p})$ is an infinite matrix of 2×2 square blocks by columns with $N_2(w_{1p})=\chi_p\begin{pmatrix} w_{11p} & -w_{21p} \\ -w_{21p} & -w_{11p} \end{pmatrix}$, $p=2t_1+1$. The usual index sum by t, $t_1=1,2,3,\cdots$ is applied.

Finally, from Eq. (27), it follows that $X_1=-(I+W)^{-1}N_2X$ and replacing into Eq. (26) results

$$\left[I + \chi_1 R_1^2 J - N_1 \left(I + W \right)^{-1} N_2 \right] X = R_1 E B \,. \tag{28}$$

Therefore, the solution of Eq. (28) is given as

$$X = R_1 E \left[I + \chi_1 \, R_1^2 J - \chi_1 N_1 \left(I + W \right)^{-1} N_2 \right]^{-1} B \,, \tag{29}$$

and this can be re-written as

$${}_{\alpha 3}a_1 = \begin{pmatrix} 1 & i \end{pmatrix} \begin{pmatrix} x_1 \\ y_1 \end{pmatrix} = R_1 E \begin{pmatrix} 1 & i \end{pmatrix} \left(I + \chi_1 \, R_1^2 J - \chi_1 N_1 \left(I + W \right)^{-1} N_2 \right)^{-1} \begin{pmatrix} \delta_{1\alpha} \\ \delta_{2\alpha} \end{pmatrix}. \tag{30}$$

Consequently, if $Z = I + \chi_1 \, R_1^2 J - \chi_1 N_1 \left(I + W \right)^{-1} N_2$ and its inverse Z^{-1} is calculated, the explicitly expression of the complex unknown coefficient ${}_{\alpha 3}a_1$ is determined, i.e.,

$${}_{13}a_1 = R_1 E \begin{pmatrix} 1 & i \end{pmatrix} Z^{-1} \begin{pmatrix} 1 & 0 \end{pmatrix}^{\mathrm{T}} = \frac{R_1 E \left(z_{22} - i z_{21} \right)}{z_{11} z_{22} - z_{12} z_{21}}, \quad \text{for the local problem } {}_{13}\mathrm{L}\,, \tag{31}$$

$${}_{23}a_1 = R_1 E \begin{pmatrix} 1 & i \end{pmatrix} Z^{-1} \begin{pmatrix} 1 & 0 \end{pmatrix}^{\mathrm{T}} = -\frac{R_1 E \left(z_{12} - i z_{11} \right)}{z_{11} z_{22} - z_{12} z_{21}}, \quad \text{for the local problem } {}_{23}\mathrm{L}\,, \tag{32}$$

where z_{11}, z_{12}, z_{21} and z_{22} are the coefficients of the matrix Z.

This methodology of solution, firstly, was used by Pobedrya (1984) in a two-phase elastic media, and next, it was applied in examples of FRC of alike systems, see for instance (Espinosa-Almeyda et al., 2017; Guinovart-Díaz et al., 2016; López-Realpozo et al., 2014), among others. This procedure allows system to be solved for first order coefficient in Laurent expansion.

From Eqs. (19) and (20), and taking into account the expression deduced from system (Eq. (22)) when $p = 1$, i.e., ${}_{\alpha 3}a_0 + \sum_{k=1}^{\infty}{}^{*}\, {}_{\alpha 3}a_k \eta_{k1} = \chi_1^{-1} \left({}_{\alpha 3}\overline{a}_1 - E R_1 \right) \left[\delta_{1\alpha} - i \delta_{2\alpha} \right]$, the equivalent analytical formulas of the antiplane effective coefficients for a periodic four-phase FRC as function of each phase volume fraction can be computed as

$$\begin{aligned} \mathrm{C}^{*}_{1313} - i\mathrm{C}^{*}_{2313} = {} & \left\langle \mathrm{C}_{1313} \right\rangle - [[\mathrm{C}_{1313}]]_2 \frac{\mathrm{V}_2 + \mathrm{V}_3 + \mathrm{V}_4}{\chi_1 R_1} \left[(1 + \chi_1) \, {}_{13}\overline{a}_1 - R_1 E \right] \\ & - [[\mathrm{C}_{1313}]]_3 \frac{\mathrm{V}_3 + \mathrm{V}_4}{R_2} \left[{}_{13}b_1^{(2)} + {}_{13}\overline{b}_{-1}^{(2)} R_1 R_2^{-1} \right] - [[\mathrm{C}_{1313}]]_4 \frac{\mathrm{V}_4}{R_3} \, {}_{13}c_1 \end{aligned}, \tag{33}$$

$$\begin{aligned} \mathrm{C}^{*}_{1323} - i\mathrm{C}^{*}_{2323} = -i\left\langle \mathrm{C}_{1313} \right\rangle - [[\mathrm{C}_{1313}]]_2 \frac{\mathrm{V}_2 + \mathrm{V}_3 + \mathrm{V}_4}{\chi_1 R_1}\left[\left(1+\chi_1\right) {}_{23}\bar{a}_1 + iR_1 E \right] \\ -[[\mathrm{C}_{1313}]]_3 \frac{\mathrm{V}_3 + \mathrm{V}_4}{R_2}\left[{}_{23}b_1^{(2)} + {}_{23}\bar{b}_{-1}^{(2)} R_1 R_2^{-1} \right] - [[\mathrm{C}_{1313}]]_4 \frac{\mathrm{V}_4}{R_3} {}_{23}c_1 \end{aligned}, \tag{34}$$

where $\left\langle \mathrm{C}_{1313} \right\rangle = \sum_{i=1}^{4} \mathrm{C}_{1313}^{(i)} \mathrm{V}_i$ is Voigt's average. Here, V_2, V_3 and V_4 are volume fractions per unit length occupied by the interphases S_2 and S_3 with radius R_1 and R_2 respectively, and by the fiber S_4 with radio R_3. The unknowns ${}_{\alpha 3}\bar{a}_1$, ${}_{\alpha 3}b_1^{(2)}$, ${}_{\alpha 3}\bar{b}_{-1}^{(2)}$ and ${}_{\alpha 3}c_1$ $(\alpha = 1,2)$ are different for each antiplane local problem ${}_{\alpha 3}\mathrm{L}$ and the expressions for determining these unknowns are summarized in Appendix B. Once these aforementioned unknowns are calculated, the antiplane effective coefficients are obtained.

Focusing on practical applications, like soft tissues, bones and so on, the general analytical solution for the antiplane local problems and the effective coefficients are adapted to periodic three-phase FRC. Therefore, the Eqs. (18)-(20) of $n-$phase elastic FRC are reduced to the case of two concentric circles in a matrix.

4.2 Solution of the antiplane local problems ${}_{\alpha 3}\mathrm{L}$ and effective properties for a three-phase FRC.

Now, the same methodology shown above is applied. Therefore, the equivalent system to Eq. (18) for $n-$phases and Eq. (22) for four-phases is defined for three-phase FRC (see Fig.2), as follows

$${}_{\alpha 3}\bar{a}_p + \chi_1 R_1^2 H_1 \delta_{1p}\, {}_{\alpha 3}\bar{a}_1 + \chi_1 R_1^2 H_2 \delta_{1p}\, {}_{\alpha 3}a_1 + \chi_p \sum_{k=1}^{\infty}{}^{*}\, {}_{\alpha 3}a_k W_{kp} = E R_1 \delta_{1p}\left[\delta_{1\alpha} - i\delta_{2\alpha}\right], \tag{35}$$

where $\chi_p = \dfrac{\left(\mathrm{V}_2+\mathrm{V}_3\right)^p \left(k_1+k_2\right)\left(1-k_1\right) + \mathrm{V}_3^p \left(k_1-k_2\right)\left(1+k_1\right)}{\left(\mathrm{V}_2+\mathrm{V}_3\right)^p \left(k_1+k_2\right)\left(1+k_1\right) + \mathrm{V}_3^p \left(k_1-k_2\right)\left(1-k_1\right)}$ and $E = \chi_1$. Here, $k_1 = \mathrm{C}_{1313}^{(2)} / \mathrm{C}_{1313}^{(1)}$, $k_2 = \mathrm{C}_{1313}^{(3)} / \mathrm{C}_{1313}^{(1)}$ and $\mathrm{V}_2\left(\mathrm{V}_3\right)$ is the interphase (central fiber) volume fraction.

Consequently, the system solution ${}_{\alpha 3}a_1$ is found by following the steps shown from Eq. (23) to Eq. (32), such as,

$${}_{13}a_1 = \frac{z_{22} - iz_{21}}{z_{11}z_{22} - z_{12}z_{21}}\chi_1 R_1 \text{ and } {}_{23}a_1 = -\frac{z_{12} - iz_{11}}{z_{11}z_{22} - z_{12}z_{21}}\chi_1 R_1, \tag{36}$$

where z_{ij} are the coefficients of matrix Z associated to the three-phase model and ${}_{\alpha 3}\bar{a}_1$ is the conjugate of ${}_{\alpha 3}a_1$.

Then, the non-null antiplane effective coefficients formulae for three-phase FRC is listed as follows

$$\mathrm{C}^*_{1313} - i\mathrm{C}^*_{2313} = \langle \mathrm{C}_{1313} \rangle - [[\mathrm{C}_{1313}]]_2 \frac{\mathrm{V}_2 + \mathrm{V}_3}{\chi_1 R_1}\left[(\chi_1 + 1)\,{}_{13}\bar{a}_1 - R_1 E\right] - [[\mathrm{C}_{1313}]]_3 \frac{\mathrm{V}_3}{R_2}\,{}_{13}c_1, \tag{37}$$

$$\mathrm{C}^*_{1323} - i\mathrm{C}^*_{2323} = -i\langle \mathrm{C}_{1313} \rangle - [[\mathrm{C}_{1313}]]_2 \frac{\mathrm{V}_2 + \mathrm{V}_3}{\chi_1 R_1}\left[(\chi_1 + 1)\,{}_{23}\bar{a}_1 + iR_1 E\right] - [[\mathrm{C}_{1313}]]_3 \frac{\mathrm{V}_3}{R_2}\,{}_{23}c_1, \tag{38}$$

where $\langle \mathrm{C}_{1313} \rangle = \mathrm{C}^{(1)}_{1313}\mathrm{V}_1 + \mathrm{C}^{(2)}_{1313}\mathrm{V}_2 + \mathrm{C}^{(3)}_{1313}\mathrm{V}_3$ is the Voigt's average and ${}_{\alpha 3}c_1$ is defined as

$${}_{\alpha 3}c_1 = \frac{k_1(\chi_1 + 1)}{\chi_1 A_{21}}\,{}_{\alpha 3}\bar{a}_1 - \frac{2k_1^2 R_1^2 E - \chi_1 k_1 (k_1 - k_2)\left(R_1^2 - R_2^2\right)}{2A_{21}\chi_1 k_1 R_1}\left[\delta_{1\alpha} - i\delta_{2\alpha}\right], \tag{39}$$

with $A_{21} = \left[R_1^2(k_1 + k_2) + R_2^2(k_1 - k_2)\right] / 2R_1R_2$.

Finally, if Eqs. (39) and (36) are replaced into Eqs. (37)-(38), the antiplane effective coefficients of a fiber coated by an interphase are achieved in simple closed-form, as follows

$$\mathrm{C}^*_{1313} = \langle \mathrm{C}_{1313} \rangle - \mathrm{C}^{(1)}_{1313}\frac{\mathrm{F}(\mathrm{V}_2 + \mathrm{V}_3)}{\chi_1 |Z|}\left[(\chi_1 + 1)z_{22} - |Z|\right] - \frac{\mathrm{C}^{(1)}_{1313}(k_1 - k_2)^2 \mathrm{V}_2\mathrm{V}_3}{(k_1 + k_2)\mathrm{V}_2 + 2k_1\mathrm{V}_3}, \tag{40}$$

$$\mathrm{C}^*_{2313} = \mathrm{C}^{(1)}_{1313}\frac{\mathrm{F}(\mathrm{V}_2 + \mathrm{V}_3)}{\chi_1}\frac{(\chi_1 + 1)z_{21}}{|Z|}, \tag{41}$$

$$\mathrm{C}^*_{1323} = \mathrm{C}^{(1)}_{1313}\frac{\mathrm{F}(\mathrm{V}_2 + \mathrm{V}_3)}{\chi_1}\frac{(\chi_1 + 1)z_{12}}{|Z|}, \tag{42}$$

$$\mathrm{C}^*_{2323} = \langle \mathrm{C}_{1313} \rangle - \mathrm{C}^{(1)}_{1313}\frac{\mathrm{F}(\mathrm{V}_2 + \mathrm{V}_3)}{\chi_1 |Z|}\left[(\chi_1 + 1)z_{11} - |Z|\right] - \frac{\mathrm{C}^{(1)}_{1313}(k_1 - k_2)^2 \mathrm{V}_2\mathrm{V}_3}{(k_1 + k_2)\mathrm{V}_2 + 2k_1\mathrm{V}_3}, \tag{43}$$

with $\mathrm{F} = \dfrac{\left[(k_1 + k_2)(1 - k_1)\mathrm{V}_2 + 2k_1(1 - k_2)\mathrm{V}_3\right]^2}{\left[(k_1 + k_2)(1 + k_1)\mathrm{V}_2 + 2k_1(1 + k_2)\mathrm{V}_3\right]\left[(k_1 + k_2)\mathrm{V}_2 + 2k_1\mathrm{V}_3\right]}$.

5. Numerical results

The broad applicability and accuracy of the results obtained from the multi-phase model by AHM is determined by comparison with others reported earlier in the literature for two-, three-, and four-phase FRC. Limit cases for the *n*-phase model can be found when Eqs. (19) and (20), and its related in Section 4, are simplified to those that represent FRC with isotropic or transversely isotropic elastic constituents and parallelogram-like unit cell, as reported in (Guinovart-Díaz et al., 2011; Rodríguez-Ramos et al., 2011).

From now on, for simplicity in the notation we use $p_\alpha = C_{1313}^{(\alpha)}$, $q_\alpha = C_{2323}^{(\alpha)}$ and $r_\alpha = C_{1323}^{(\alpha)} = C_{2313}^{(\alpha)}$, and the effective properties $p = C_{1313}^{*}$, $q = C_{2323}^{*}$ and $r = C_{1323}^{*} = C_{2313}^{*}$.

a) *Four-phase FRC.*

Eqs. (33) and (34) for four-phase FRC with perfect contact condition at interfaces and parallelogram unit cell are now used to study the interesting interphase properties combination effect on effective shears.

Figs. 3 and 4 show plots of effective dimensionless shear moduli p/p_1, q/p_1 and r/p_1 as a function of $\log(p_3/p_1)$ for four-phase FRC with either a hard or soft p_2/p_1 interphase and a parallelogram unit cell of $\theta = 45^o$. Material properties are taken from (Dasgupta and Bhandarkar, 1992). In both figures $p_4/p_1 = 1.62$ and volume interphase fractions are set to $V_2 = V_3 = 0.1$, $V_4 = 0.4$, while in Fig. 3 a hard interphase $p_2/p_1 = 11.22$ is considered; on the other hand, a softer interphase $p_2/p_1 = 0.1122$ is analyzed in Fig. 4. Let us analyze initially Fig. 3. It brings to notice that an effective isotropic behavior is induced for low p_3/p_1 values, that is, $p = q$ and $r = 0$. In contrast, an effective anisotropic behavior is displayed for high p_3/p_1 values, that is, the properties differ noticeably so that $p_1 < p < q$, $r < 0$. The opposite behavior, however, occurs in Fig. 4, i.e., an effective anisotropic behavior instead arises for low p_3/p_1 values, that is, $p_1 < p < q$, $r < 0$. When p_3/p_1 increases, the effective medium becomes isotropic. In conclusion, this radical change between isotropic and anisotropic effective behaviors in the

composite is due to the exchange of p_2 / p_1 from a hard to a soft interphase and low and high p_3 / p_1 values.

Fig. 3

Fig. 4

Formulas Eqs. (32) and (33) are here applied to analyze the effect of empty fiber on effective properties of a two-phase FRC with complex constituent properties and several parallelogram unit cells.

Firstly let us consider that the periodicity is square $(\theta = 90^o)$ and hexagonal $(\theta = 60^o)$. Here, effective complex shear properties p, q and r are calculated considering that the interphases and matrix volume fractions are given as $V_2 = V_3 = 10^{-8}$ and $V_1 = 1 - 2V_2 - V_4$ which are convenient for our purposes. Hence, the void fiber has a very high-volume concentration close to the central fiber volume fraction V_4. Also, the matrix constituent material is complex and isotropic, i.e., $p_1 = 30 - 0.5i$ GPa whereas isotropic interphases (p_2, p_3) and fiber (p_4) are set equal to 10^{-6} GPa. Calculation results are shown in Table 1. It displays p, q and r as a function of V_4 from $V_4 = 0$ to $V_4 = 0.7$ when $\theta = 90^o$ and $\theta = 60^o$. It can be seen that composite's effective behavior is isotropic for both fiber distributions, that is, $p = q$ and complex, and $r = 0$. Also, both real and imaginary parts of p decrease monotonically as the void volume fraction V_4 increases. This weakening effect is due to the pore size increase. It is worthwhile to note that the effective shear complex properties for both arrays are very close to each other. It is important to mention that (Jiang et al., 2004) in Table 7 carry out calculations for transversely isotropic porous media with both fiber distributions and matrix real properties. The relevant one for our purpose here is $\Re(p_1)$. Good agreement is obtained between the real part of the effective shear complex properties and the results reported by (Jiang et al., 2004) for all V_4 and both arrays.

Table 1

The effective complex shear properties p, q and r for two-phase FRC with parallelogram unit cell of $\theta = 45^o$ and $\theta = 75^o$ are shown in Table 2. Here, p, q and r are found considering the same material parameters as Table 1. Note that composite's effective behavior is monoclinic for both fiber distributions, that is, $p \neq q$ and complex, and $r \neq 0$. In addition, it can be observed that spatial fiber distribution has a significant effect on composite behavior, that is, the real and imaginary parts of r show noticeably differences from one angle to another.

Table 2

b) *Three-phase FRC*

In this section, four examples are chosen to show the usefulness of Eqs. (40)-(43) to compute effective complex transport properties of periodic two- and three-phase FRC.

Example 1) Now, real and imaginary parts of the effective complex permittivities p, q and r versus fiber volume fraction V_3 are plotted for two-phase FRC with square $(\theta = 90^o)$ (see Fig. 5), hexagonal $(\theta = 60^o)$ (see Fig. 6) and parallelogram $(\theta = 67.5^o)$ (see Fig. 7) unit cells. Herein, p, q and r are derived using Eqs. (40)-(43) considering that $V_2 = 0$ so that the matrix volume fraction is $V_1 = 1 - V_3$. The constituent materials of matrix (p_1) and fiber (p_3) have isotropic complex dielectric properties, such as: $p_1 = 1 - 5i$, $p_3 = 30 - 0.3i$ (composite A) and $p_1 = 2 - 0.3i$, $p_3 = 1 - 8i$ (composite B). We remark that square or hexagonal fiber distributions induce an isotropic effective behavior, that is, $p = q$ and $r = 0$ (as in Figs. 5 and 6) whereas parallelogram unit cell of $\theta = 67.5^o$ brings a monoclinic effective behavior, $p \neq q$ and $r \neq 0$ (as in Fig. 7).
The results displayed on the top two boxes in Fig. 5 and 6 refer to composite A whereas the two bottom ones to composite B. In Fig. 5, the real and imaginary parts of the effective complex permittivity p, $\Re(p)$ and $\Im(p)$, respectively, exhibits interesting different behavior for both composites. $\Re(p)$ corresponding to composite A is a monotone increasing and convex function; also, it reaches its highest value near to close-packing condition. On the other hand, for the composite B it is worthwhile to mention that $\Re(p)$ has an inflexion point and also is larger than

the constituent's real part in the whole interval. Besides, as V_3 increases, $\Re(p)$ reaches its maximum value near to 3.67 at $V_3 \approx 0.57$ and then begins to weaken rapidly until the close-packing condition. Otherwise, a different behavior is observed relative to imaginary parts. $\Im(p)$ corresponding to composite A has an inflexion point and also is smaller than the imaginary part of the constituents in the whole interval. Besides, as V_3 increases, $\Im(p)$ attains its minimum value about -11.82 at $V_3 \approx 0.63$ and then begins to increase up to close-packing condition. Then, for the composite B, $\Im(p)$ is a monotone decreasing and convex function.

A similar tendency is observed in Fig. 6 for a hexagonal array except that the maximum value of $\Re(p)$ for composite B is near to 3.81 at $V_3 \approx 0.63$ and the minimum value of $\Im(p)$ for composite A is near to -12.65 at $V_3 \approx 0.69$. In both figures, the AHM results are compared with those reported by (Godin, 2013) up to close-packing conditions. Excellent agreement between both methods is observed. Figs 5 and 6 also show upper (UB H-S) and lower (LB H-S) Hashin and Shtrikman bounds for complex permittivity (Milton, 1980). In addition, it can be seen that the results of both, AHM and Godin, methods are always located within the bounds of (Hashin and Shtrikman, 1962). Fig. 7 displays results related to composite A. It can be noticed that, good agreement in general is observed between AHM and Godin (2013) for p and q in the whole interval of V_3. However, an important discrepancy is observed for r. As far as it can be seen the difference between the results of r is probably due to the system truncation order of both methods. In addition, the phenomena of gain/loss enhancement in dielectrics are noted in Figs. 5-7.

Fig. 5

Fig. 6

Fig. 7

Example 2) Here, Eqs. (40)-(43) are applied to calculate effective dielectric properties of periodic three-phase FRC with square (Figs. 8) and hexagonal (Figs. 9) arrays. The complex-

values of matrix, interphase and fiber properties of which are taken from Godin (2016), such as $\mathrm{p}_1 = 5 - 4i$, $\mathrm{p}_2 = 80 - 2i$ and $\mathrm{p}_3 = 2 - 4i$ for square array and $\mathrm{p}_1 = 1$, $\mathrm{p}_2 = 8 - 40i$ and $\mathrm{p}_3 = 2 - 4i$ for hexagonal array, respectively. Figs. 8 and 9 show the real and imaginary parts of complex effective isotropic dielectric properties p, $\Re(\mathrm{p})$ and $\Im(\mathrm{p})$, respectively, as a function of normalized radius $h = R_1 / l$, $h \leq 1/2$, where R_1 is outer interface radius and l is the least distance between the centers of the fibers.

Fig. 8 displays that $\Re(\mathrm{p})$ is a monotone increasing and convex function in the whole interval whereas $\Im(\mathrm{p})$ reaches lower values than the constituent properties and in contrast has an inflection point, like the behavior present in two-phase FRC, as in Fig. 5 and 6. In Fig. 9, a different behavior is present. Here, the result of three-phase model (AHM) are compared with those ones reported by (Godin, 2016) showing a small discrepancy near to the close-packing condition for a hexagonal array. In both figures, good approximations are displayed.

Fig. 8

Fig. 9

Example 3) The application of the present model to biological tissue is of great interest. In particular tissues that are made of growing and non-growing components. Then, an application of composites into tissue mechanics is here studied. For that, Eqs. (40)-(43) have been derived under the hypothesis that material ratios $\mathrm{p}_2 / \mathrm{p}_1$, $\mathrm{p}_3 / \mathrm{p}_1$ and interphase properties are real quantities. However, constituent materials and effective properties are complex numbers in general, see for instance (Perrins et al., 1979).

Three-phase FRC models can be a suitable idealization of biological tissue comprising tubular cells, such as skeletal muscle. A cell is surrounded by its plasma membrane, which it is made of dielectric lipid bilayers. Therefore, plasma membrane can be represented as a two-dimensional interfaces in which conductance and capacitance per unit area are given by bilayer conductivity and permittivity, respectively, and divided by its thickness *h*, see (Bisegna and Caselli, 2008).

In this case, effective complex conductivity p, q and r of a biological specimen (skeletal muscle) with interfacial impedance K studied in (Bisegna and Caselli, 2008) for a two-phase composite,

are calculated here using a variant of AHM for a three-phase FRC (Eq. (40)-(43)) with a very thin interphase via Hashin's approximation (Hashin, 2001; 2002). Herein, interfacial admittance per unit area is defined as $K = B + i\omega C$, where $B(C)$ is conductance (capacitance) per unit area and ω is circular frequency. A very thin interphase admittance caused by electric potential jump across interfaces can be referred to as an imperfect interface as well as imperfect impedance interface (Bisegna and Caselli, 2008). The relationship between K and the interphase property p_2 is $K = p_2 R_2 / h$ with $h = 10^{-4}$ as in (Hashin, 2001; 2002), according to the present three-phase model.

Figs. 10 (a) – (b) and Fig. 11 plots normalized real and imaginary parts of the effective complex conductivities p, q and r versus dimensionless circular frequency Ω, $\Omega = \omega C L / p_2$, where L is the microstructural dimension of the composite. Three parallelogram unit cells of $\theta = 45^o, 50^o$ and 60^o are considered and p_1 is the matrix conductivity. For the computations, the material ratio is satisfied $p_3 / p_1 = 0.25$ and the interphase fiber and matrix volume fractions are $V_2 = 32 \times 10^{-4}$, $V_3 = 0.62$ and $V_1 = 1 - V_2 - V_3$. Also, a comparison with the results obtained by (Bisegna and Caselli, 2008) (red circles, BC) and this paper (asterisk) is shown for a isotropic composite with hexagonal unit cell. Excellent agreement is obtained.

From Fig. 10 and 11, it is concluded that the composite has an isotropic behavior when a hexagonal unit cell of $\theta = 60^o$ is considered, whereas it has a monoclinic one for parallelogram unit cells of $\theta = 45^o$ (denoted by squares) and $\theta = 50^o$ (denoted by triangles). Fig. 10(c) displays imaginary parts of dimensionless effective permittivities $\left(\Im(p)/(p_1\Omega), \Im(q)/(p_1\Omega)\right)$ as a function of Ω and Fig. 10(d) shows normalized imaginary parts $\left(\Im(p)/p_1, \Im(q)/p_1\right)$ versus normalized real parts $\left(\Re(p)/p_1, \Re(q)/p_1\right)$ of effective complex conductivities p and q. In addition, as shown in Fig. 11, normalized real part of r, $\Re(r)/p_1$, exhibits an increasing monotonic behavior for all Ω, moreover, normalized imaginary part $\Im(r)/p_1$ attains a maximum value. The novelty of this contribution in comparison with the results reported by (Bisegna and Caselli, 2008) is the fiber distribution effect on the effective complex conductivities. This result revealed that a small change in periodicity of composite induces a

different global behavior of effective complex conductivity. It provides information about optimal design of composites.

Although this example considers electrical conductivity its results easily translates into the elastic realm, that is, in a three-phase FRC, a very thin interphase models very well, via the well-known Hashin's approximation, the so-called imperfect condition at the interface in an elastic two-phase FRC.

Fig. 10

Fig. 11

Example 4) From now, the problem of enhancement of the homogenized quasi-static effective mass densities p is analyzed by means of the three-phase model. The theoretical phenomenon of enhanced permittivity with electromagnetic waves using lossy materials is studied by Guild et al. (2014) as applied to mass density and so that acoustic waves representing inertial enhancements. In that work, the fundamental results of Godin (2013) are adapted to acoustics when the frequency $\omega \to 0$ and then, they are used to find the effective mass density of fluid cylinders in the quasi-static limit.

Therefore, Eq. (39)-(42) are used to calculate the quasi-static effective mass densities p, q and r of a FRC with fluid constituents. Here, the matrix phase and inclusions (interphase and fiber phases, respectively) occupy the regions S_1, S_2 and S_3, in that order (see Fig. 2(a)). In the theoretical model developed by (Guild et al., 2014), the case of FRC with multi-fiber inclusions embedded into a matrix is not considered.

Fig. 12 illustrates the enhancement of the real part of p, $\Re(\mathrm{p})$, for a composite with different annular inclusions and hexagonal unit cell $(\theta = 60^{\circ})$ as function of reduced filling fraction V_2 (discontinues lines). Here, an enhancement of p is obtained when the annular inclusions have a fixed fraction $\mathrm{V}_2 + \mathrm{V}_3$ in each configuration and filling fraction. In addition, the effective mass density augmentation can be observed in comparison with the effective mass density of a composite with a circular fluid inclusion reported in (Guild et al., 2014) (solid line). For this example, the matrix and inclusions have complex densities, such as: $\mathrm{p}_1 = \mathrm{p}_3 = 1 - i$ and

$p_2 = 0.99 - 0.5i$ (Fig. 12(a)) or $p_2 = 1.01 - 0.5i$ (Fig. 12(b)). They are chosen so that they attain an interval of realistic physical properties (Guild et al., 2014).

From Fig. 12, it is remarked that, the case $V_3 = 0$ reproduces the results reported in Fig. 3(c) and (d) of (Guild et al., 2014) (solid line). When $0 < V_3 < 1$, the result shows an enhancement of $\Re(p)$ as a function of V_2. Besides, $\Re(p)$ increases as the fluid inclusions volume fraction $V_2 + V_3$ increases. From the numerical experiments we can conclude that imaginary part values vary monotonically between the bounds of the host fluid and fluid inclusions values and the real part values exceed the bounds of either of the individual components and even the composite without interphase, i.e., $V_3 = 0$. Here, the red dashdot line represents the value of the real part of host fluid p_1 and the blue dashed line the corresponding to fluid inclusion p_2.

Fig. 12

Conclusions

Effective properties of periodic multi-phase fiber-reinforced composites with complex-valued constituents transport properties and parallelogram unit cells are found by means of the two-scale asymptotic homogenization method. The general analytical formulae of antiplane local problems and associated effective shear properties are derived for a $n-$ phase fiber-reinforced composites. It is required to solve a convergent normal infinite system of equations. It leads to simple closed-form formulas are obtained for three- and four-phase fiber-reinforced composites.

Based on the numerical results, the following conclusions can be drawn:

i) Macroscopically, the effect of the fiber spatial distributions on the complex effective behavior induces three point group symmetry classes: tetragonal 4mm (square cell), hexagonal 6mm (hexagonal cell) and monoclinic (other parallelogram cells). It also pertains to real and imaginary parts as well.
ii) Increasing porosity produces a weaker composite. It confirms a well-known result.
iii) A radical change from isotropic to anisotropic effective behavior is observed in a four-phase composite when one interphase is hard and the other one varies from a softer material to a harder one, while matrix and fiber properties and all volume fractions are fixed. The opposite

takes place when former interphase is soft, that is, the composite effective behavior changes from anisotropic to isotropic, see Figs. 3 and 4.

iv) A three-phase FRC with a very thin interphase provides indeed a very good estimation for effective conductivity of biological specimens with imperfect interfacial impedance via Hashin's approximation.

v) In the case of three-phase FRC with fluid constituents, it is found that both real and imaginary parts of effective mass density may be slightly enhance relative to two-phase FRC by the addition of an interphase where the constituents mass properties are chosen so that they attain an interval of realistic physical properties.

The broad applicability and efficiency of the present model are tested against results obtained using other methods for periodic two-, three and four-phase fiber-reinforced composites. Good agreement is obtained. Formulas may be useful as benchmarks for checking experimental and numerical results.

Acknowledgements

YE gratefully acknowledges the Program of Postdoctoral Scholarships of DGAPA from UNAM, México. RG and RR would like to thank to COIC/STIA/ 9042 and COIC/STIA/9045/2019. RR thanks the International Research Training Group GRK 2078 "Integrated engineering of continuous-discontinuous long fiber reinforced polymer structures" (CoDiCoFRP) funded by German Research Foundation (DFG) for inviting him as a guest scientist, parts of the manuscript were written during this stay. JB and FJS acknowledge the funding of PAPIIT-DGAPA-UNAM IA100919. TB acknowledges the support by DFG under the grant GRK 2078/2. Thanks to the Department of Mathematics and Mechanics, IIMAS-UNAM, for its support and Ramiro Chávez Tovar and Ana Pérez Arteaga for computational assistance.

Conflicts of Interest: The authors declare no conflict of interest.

Appendix A

The magnitudes involved in the system Eq. (22) are summarized

$$\chi_p = \frac{A_{2p} - k_1 A_{1p}}{A_{2p} + k_1 A_{1p}}, \tag{A.1}$$

$$A_{1p} = D_p \begin{bmatrix} (k_1+k_2)(k_2+k_3)R_1^{2p}R_2^{2p} + (k_1-k_2)(k_2-k_3)R_1^{2p}R_3^{2p} \\ -(k_1-k_2)(k_2+k_3)R_2^{4p} - (k_1+k_2)(k_2-k_3)R_2^{2p}R_3^{2p} \end{bmatrix}, \tag{A.2}$$

$$A_{2p} = D_p \begin{bmatrix} (k_1+k_2)(k_2+k_3)R_1^{2p}R_2^{2p} + (k_1-k_2)(k_2-k_3)R_1^{2p}R_3^{2p} \\ +(k_1-k_2)(k_2+k_3)R_2^{4p} + (k_1+k_2)(k_2-k_3)R_2^{2p}R_3^{2p} \end{bmatrix}, \tag{A.3}$$

$$D_p = \frac{1}{4k_2 R_1^p R_2^{2p} R_3^p}, \text{ and } E = \frac{\begin{bmatrix} R_1^2(1-k_1)\left[(k_1-k_2)(k_2-k_3)R_3^2 + (k_1+k_2)(k_2+k_3)R_2^2\right] \\ +R_2^2(1+k_1)\left[(k_1+k_2)(k_2-k_3)R_3^2 + (k_1-k_2)(k_2+k_3)R_2^2\right] \end{bmatrix}}{\begin{bmatrix} R_1^2(1+k_1)\left[(k_1-k_2)(k_2-k_3)R_3^2 + (k_1+k_2)(k_2+k_3)R_2^2\right] \\ +R_2^2(1-k_1)\left[(k_1+k_2)(k_2-k_3)R_3^2 + (k_1-k_2)(k_2+k_3)R_2^2\right] \end{bmatrix}}. \tag{A.4}$$

Appendix B

The expressions used to determine the unknown coefficients ${}_{\alpha 3}b_1^{(2)}$, ${}_{\alpha 3}\bar{b}_{-1}^{(2)}$ and ${}_{\alpha 3}c_1$ involved in the effective coefficients Eqs. (33)-(34) are given as follows:

$$\begin{aligned} {}_{\alpha 3}b_1^{(2)} &= \frac{(k_1+k_2)(k_2+k_3)R_2^2 + (k_1-k_2)(k_2-k_3)R_3^2}{4k_1k_2R_2R_3}\,{}_{\alpha 3}c_1 \\ &+ \frac{(k_1-k_2)(k_2-k_3)R_3^2 - \left[(k_1+k_2)(k_2-k_3) + 2k_2(k_1-k_2)\right]R_2^2}{4k_1k_2R_2}\left[\delta_{1\alpha} - i\delta_{2\alpha}\right] \end{aligned}, \tag{B.1}$$

$$\begin{aligned} {}_{\alpha 3}\bar{b}_{-1}^{(2)} &= \frac{(k_1-k_2)(k_2+k_3)R_2^2 + (k_1+k_2)(k_2-k_3)R_3^2}{4k_1k_2R_1R_3}\,{}_{\alpha 3}c_1 \\ &+ \frac{(k_1+k_2)(k_2-k_3)R_3^2 + (k_1-k_2)(k_2+k_3)R_2^2}{4k_1k_2R_1}\left[\delta_{1\alpha} - i\delta_{2\alpha}\right] \end{aligned}, \tag{B.2}$$

$${}_{\alpha 3}c_1 = \frac{k_1}{A_{21}}\,{}_{\alpha 3}\bar{a}_1 + \left\{\frac{k_1\chi_1}{A_{21}}\left[{}_{\alpha 3}\bar{a}_1 - R_1E\right] - \frac{G}{4k_2R_1R_2^2A_{21}}\right\}\left[\delta_{1\alpha} - i\delta_{2\alpha}\right], \text{ and} \tag{B.3}$$

$$\begin{aligned} G &= (k_2-k_3)\left[(k_1-k_2)R_1^2R_3^2 + (k_1+k_2)R_2^2R_3^2 - (k_1+k_2)R_1^2R_2^2 - (k_1-k_2)R_2^4\right] \\ &+ 2k_2(k_1-k_2)\left(R_2^4 - R_1^2R_2^2\right) \end{aligned}. \tag{B.4}$$

References

Ahmadi, M., Ansari, R., Hassanzadeh-Aghdam, M.K., 2019. Finite element analysis of thermal conductivities of unidirectional multiphase composites. Composite Interfaces 26, 1035-1055.

Bakhvalov, N.S., Panasenko, G.P., 1989. Homogenization Averaging Processes in Periodic Media. Kluwer Academic, Dordrecht.

Beicha, D., Kanit, T., Brunet, Y., Imad, A., Moumen, A.E., Khelfaoui, Y., 2016. Effective transverse elastic properties of unidirectional fiber reinforced composites. Mechanics of Materials 102, 47-53.

Bisegna, P., Caselli, F., 2008. A simple formula for the effective complex conductivity of periodic fibrous composites with interfacial impedance and applications to biological tissues. Journal of Physics D: Applied Physics 41, 115506.

Bonfoh, N., Coulibaly, M., Sabar, H., 2014. Effective properties of elastic composite materials with multi-coated reinforcements: A new micromechanical modelling and applications. Composite Structures 115, 111-119.

Dasgupta, A., Bhandarkar, S.M., 1992. A generalized self-consistent Mori-Tanaka scheme for fiber-composites with multiple interphases. Mechanics of Materials 14, 67 - 82.

Dinzart, F., Sabar, H., Berbenni, S., 2016. Homogenization of multi-phase composites based on a revisited formulation of the multi-coated inclusion problem. International Journal of Engineering Science 100, 136-151.

Eshelby, J.D., 1957. The determination of the elastic field of an ellipsoidal inclusion, and related problems. Proceedings of the Royal Society of London Series A 241, 376-396.

Espinosa-Almeyda, Y., Camacho-Montes, H., Rodríguez-Ramos, R., Guinovart-Díaz, R., López-Realpozo, J.C., Bravo-Castillero, J., Sabina, F.J., 2017. Influence of imperfect interface and fiber distribution on the antiplane effective magneto-electro-elastic properties for fiber reinforced composites. International Journal of Solids and Structures 112, 155-168.

Giraud, A., Sevostianov, I., Kushch, V.I., Cosenza, P., Prêt, D., Barthélémy, J.F., Trofimov, A., 2019. Effective electrical conductivity of transversely isotropic rocks with arbitrarily oriented ellipsoidal inclusions. Mechanics of Materials 133, 174-192.

Godin, Y.A., 2012. The effective conductivity of a periodic lattice of circular inclusions. Journal of Mathematical Physics 53, 063703.

Godin, Y.A., 2013. Effective complex permittivity tensor of a periodic array of cylinders. Journal of Mathematical Physics 54, 053505.

Godin, Y.A., 2016. Effective properties of periodic tubular structures. Quarterly Journal of Mechanics and Applied Mathematics 69, 181-193.

Grigolyuk, E.I., Fil'shtinskii, L., 1970. Perforated plates and shells. M.: Nauka.

Guild, M.D., Garcia-Chocano, V.M., Kan, W., Sánchez-Dehesa, J., 2014. Enhanced inertia from lossy effective fluids using multi-scale sonic crystals. AIP Advances 4, 124302.

Guinovart-Díaz, R., Bravo-Castillero, J., Rodríguez-Ramos, R., Sabina, F.J., 2001. Closed-form expressions for the effective coefficients of fibre-reinforced composite with transversely isotropic constituents. I: Elastic and hexagonal symmetry. Journal of Mechanics Physics of Solids 49, 1445-1462.

Guinovart-Díaz, R., López-Realpozo, J.C., Rodríguez-Ramos, R., Bravo-Castillero, J., Ramírez, M., Camacho-Montes, H., Sabina, F.J., 2011. Influence of parallelogram cells in the axial behaviour of fibrous composite. International Journal of Engineering Science 49, 75-84.

Guinovart-Díaz, R., Rodríguez-Ramos, R., Bravo-Castillero, J., López-Realpozo, J.C., Sabina, F.J., Sevostianov, I., 2013. Effective elastic properties of a periodic fiber reinforced composite with parallelogram-like arrangement of fibers and imperfect contact between matrix and fibers. International Journal of Solids and Structures 50, 2022-2032.

Guinovart-Díaz, R., Rodríguez-Ramos, R., Bravo-Castillero, J., Sabina, F.J., Otero-Hernández, J.A., Maugin, G.A., 2005. A recursive asymptotic homogenization scheme for multi-phase fibrous elastic composites. Mechanics of Materials 37, 1119-1131.

Guinovart-Díaz, R., Rodríguez-Ramos, R., López-Realpozo, J.C., Bravo-Castillero, J., Otero, J.A., Sabina, F.J., Lebon, F., Dumont, S., 2016. Analysis of fibrous elastic composites with nonuniform imperfect adhesion. Acta Mechanica 227, 57-73.

Görthofer, J., Meyer, N., Pallicity, T.D., Schöttl, L., Trauth, A., Schemmann, M., Hohberg, M., Pinter, P., Elsner, P., Henning, F., Hrymak, A., Seelig, T., Weidenmann, K., Kärger, L., Böhlke, T., 2019. Virtual process chain of sheet molding compound: Development, validation and perspectives. Composites Part B: Engineering 169, 133-147.

Hashin, Z., 2001. Thin interphase/imperfect interface in conduction. Journal of Applied Physics 89, 2261-2267.

Hashin, Z., 2002. Thin interphase/imperfect interface in elasticity with application to coated fiber composites. Journal of the Mechanics and Physics of Solids 50, 2509 - 2537.

Hashin, Z., Shtrikman, S., 1962. A Variational Approach to the Theory of the Effective Magnetic Permeability of Multiphase Materials. Journal of Applied Physics 33, 3125-3131.

Hassan, S.A., Ahmed, H., Israr, A., 2013. An Analytical Modeling for Effective Thermal Conductivity of Multi-Phase Transversely Isotropic Fiberous Composites Using Generalized Self-Consistent Method. Applied Mechanics and Materials 249-250, 904-909.

Jiang, C.P., Xu, Y.L., Cheung, Y.K., Lo, S.H., 2004. A rigorous analytical method for doubly periodic cylindrical inclusions under longitudinal shear and its application. Mechanics of Materials 36, 225-237.

Kaddouri, W., El Moumen, A., Kanit, T., Madani, S., Imad, A., 2016. On the effect of inclusion shape on effective thermal conductivity of heterogeneous materials. Mechanics of Materials 92, 28-41.

Kantorovich, L.V., Krylov, V.I., 1964. Approximate methods of higher analysis, 3rd ed. Interscience, INC-New York, P. Noordhoff LTD-Groningen, The Netherlands.

Kolpakov, A., Kolpakov, A., 2009. Capacity and Transport in Contrast Composite Structures: asymptotic analysis and applications, 1st ed. CRC Press, Boca Raton.

Lee, Y.-M., Yang, R.-B., Gau, S.-S., 2006. A generalized self-consistent method for calculation of effective thermal conductivity of composites with interfacial contact conductance. International Communications in Heat and Mass Transfer 33, 142-150.

Lu, J.-K., 1994. Boundary Value Problems for Analytic Functions.

López-Realpozo, J.C., Rodríguez-Ramos, R., Guinovart-Díaz, R., Bravo-Castillero, J., Otero, J.A., Sabina, F.J., Lebon, F., Dumont, S., Sevostianov, I., 2014. Effective elastic shear stiffness of a periodic fibrous composite with non-uniform imperfect contact between the matrix and the fibers. International Journal of Solids and Structures 51, 1253-1262.

López-Realpozo, J.C., Rodríguez-Ramos, R., Guinovart-Díaz, R., Bravo-Castillero, J., Sabina, F.J., 2011. Transport properties in fibrous elastic rhombic composite with imperfect contact condition. International Journal of Mechanical Sciences 53, 98-107.

Mackay, T.G., Lakhtakia, A., 2016. Gain and loss enhancement in active and passive particulate composite materials. Waves in Random and Complex Media 26, 553–563.

McCullough, R.L., 1985. Generalized combining rules for predicting transport properties of composite materials. Composites Science and Technology 22, 3-21.

Milton, G.W., 1980. Bounds on the complex dielectric constant of a composite material. Applied Physics Letters 37, 300-302.

Müller, V., Brylka, B., Dillenberger, F., Glöckner, R., Kolling, S., Böhlke, T., 2016. Homogenization of elastic properties of short-fiber reinforced composites based on measured microstructure data. Journal of Composite Materials 50, 297-312.

Müller, V., Kabel, M., Andrä, H., Böhlke, T., 2015. Homogenization of linear elastic properties of short-fiber reinforced composites – A comparison of mean field and voxel-based methods. International Journal of Solids and Structures 67-68, 56-70.

Nemat-Nasser, S., Hori, M., 1993. Micromechanics: Overall Properties of Heterogeneous Materials. Academic Press, Elsevier.

Otero, J.A., Rodríguez-Ramos, R., Bravo-Castillero, J., Guinovart-Díaz, R., Sabina, F.J., Monsivais, G., 2013. Semi-analytical method for computing effective properties in elastic composite under imperfect contact. International Journal of Solids and Structures 50, 609-622.

Pal, R., 2014. Electromagnetic, Mechanical, and Transport Properties of Composite Materials, 1st ed. CRC Press, Boca Raton.

Palla, P.L., Stefano, G., 2016. Transport properties of multigrained nanocomposites with imperfect interfaces. Journal of Applied Physics 120, 184301.

Perchikov, N., Aboudi, J., 2017. The response of conductive-fiber reinforced composites to electric field. International Journal of Engineering Science 116, 35-57.

Perrins, W., McKenzie, D., McPhedran, R., 1979. Transport Properties of Regular Arrays of Cylinders. Proceedings of The Royal Society A: Mathematical, Physical and Engineering Sciences 369, 207-225.

Pobedrya, B.E., 1984. Mechanics of Composite Materials. Moscow State University Press (in Russian).

Rodríguez-Ramos, R., Sabina, F.J., Guinovart-Díaz, R., Bravo-Castillero, J., 2001. Closed-form expressions for the effective coefficients of a fiber-reinforced composite with transversely isotropic constituents–I. Elastic and square symmetry. Mechanics of Materials 33, 223-235.

Rodríguez-Ramos, R., Berger, H., Guinovart-Díaz, R., López-Realpozo, J.C., Würkner, M., Gabbert, U., Bravo-Castillero, J., 2012. Two approaches for the evaluation of the effective properties of elastic composite with parallelogram periodic cells. International Journal of Engineering Science 58, 2-10.

Rodríguez-Ramos, R., Yan, P., López-Realpozo, J.C., Guinovart-Díaz, R., Bravo-Castillero, J., Sabina, F.J., 2011. Two analytical models for the study of periodic fibrous elastic composite with different unit cells. Composite Structures 93, 709 - 714.

Sevostianov, I., Rodríguez-Ramos, R., Guinovart-Díaz, R., Bravo-Castillero, J., Sabina, F.J., 2012. Connections between different models describing imperfect interfaces in periodic fiber-reinforced composites. International Journal of Solids and Structures 49, 1518 - 1525.

Yan, P., Zhang, Z.A., Chen, F.L., Jiang, C.P., Wang, X.J., Qiu, Z.P., 2018. Effective transport properties of composites with a doubly-periodic array of fiber pairs and with a triangular array of fibers. ZAMM - Journal of Applied Mathematics and Mechanics / Zeitschrift für Angewandte Mathematik und Mechanik 98, 312-329.

Figure caption

Fig. 1 Periodic multi-phase FRC and its corresponding parallelogram-like unit cell Y.

Fig. 2 Parallelogram-like unit cells: (a) three-phase and (b) four-phase FRC.

Fig. 3 Dimensionless effective shear moduli as a function of $\log(p_3/p_1)$ with a hard interphase p_2/p_1.

Fig. 4 As in Fig.3 but for a soft interphase p_2/p_1.

Fig. 5 Real and imaginary parts of effective complex permittivity $p=q$ for a two-phase FRC with square unit cell. Hashin-Shtrikman upper and lower bounds are shown.

Fig. 6 Real and imaginary parts of the effective complex permittivity $p=q$ for a two-phase FRC with hexagonal unit cell. Hashin-Shtrikman upper and lower bounds are displayed.

Fig. 7 Real and imaginary parts of the effective complex permittivities p, q and r for a two-phase FRC with parallelogram unit cell of $\theta=67.5^o$ for AHM and Godin's technique.

Fig. 8 Real and imaginary parts of the complex effective dielectric property p for a three-phase FRC with square unit cell.

Fig. 9 Same as Fig. 8 except that the array is hexagonal.

Fig. 10 Normalized real and imaginary parts of effective complex conductivities p and q versus dimensionless circular frequency for different parallelogram unit cells.

Fig. 11 Normalized real and imaginary parts of effective complex coefficient r versus dimensionless circular frequency for two parallelogram unit cells of $\theta=45^o$ and $\theta=50^o$.

Fig. 12 Enhancement of the real part of effective mass density p as function of filling fraction V_2 for a composite with annular inclusions (black discontinues lines) and hexagonal unit cell related to a composite with circular fluid inclusion (black solid line).

Table caption

Table 1. Porosity effect on effective shear complex moduli of two-phase FRC with square and hexagonal unit cell.

Table 2. As in Table 1 but for parallelogram unit cells of $\theta = 45^{o}$ and $\theta = 75^{o}$.

Table(s)

Table 1

V_4	Effective shear complex properties (GPa) (square unit cell, $\theta = 90^o$)			Effective shear complex properties (GPa) (hexagonal unit cell, $\theta = 60^o$)		
	p	r	q	p	r	q
0	30–0.5*i*	0	30-0.5*i*	30–0.5*i*	0	30-0.5*i*
0.1	24.5453–0.40909*i*	0	24.5453–0.40909*i*	24.5455–0.40909*i*	0	24.5455–0.40909*i*
0.2	19.9959–0.33327*i*	0	19.9959–0.33327*i*	20.0000–0.33333*i*	0	20.0000–0.33333*i*
0.3	16.1274–0.26879*i*	0	16.1274–0.26879*i*	16.1533–0.26922*i*	0	16.1533–0.26922*i*
0.4	12.7605–0.21268*i*	0	12.7605–0.21268*i*	12.8534–0.21422*i*	0	12.8534–0.21422*i*
0.5	9.73964–0.16233*i*	0	9.73964–0.16233*i*	9.98427–0.16641*i*	0	9.98427–0.16641*i*
0.6	6.90954–0.11516*i*	0	6.90954–0.11516*i*	7.45029–0.12417*i*	0	7.45029–0.12417*i*
0.7	4.03621–0.06727*i*	0	4.03621–0.06727*i*	5.16251–0.08604*i*	0	5.16251–0.08604*i*

Table 2

V_4	Effective shear complex properties (GPa) (parallelogram unit cell of $\theta = 45^o$)		
	p	r	q
0	30–0.5*i*	0	30–0.5*i*
0.1	24.444–0.4074*i*	–0.0981+0.0016*i*	24.640–0.4107*i*
0.2	19.645–0.3274*i*	–0.3303+0.0055*i*	20.305–0.3384*i*
0.3	15.438–0.2573*i*	–0.6367+0.0106*i*	16.711–0.2785*i*
0.4	11.674–0.1946*i*	–0.9893+0.0165*i*	13.653–0.2276*i*
0.5	8.1810–0.1364*i*	–1.3959+0.0233*i*	10.973–0.1829*i*
0.6	4.5681–0.0761*i*	–1.9732+0.0329*i*	8.5146–0.1419*i*
0.7	3.7916–0.0632*i*	–1.4675+0.0245*i*	6.7267–0.1121*i*
V_4	Effective shear complex properties (GPa) (parallelogram unit cell of $\theta = 75^o$)		
	p	r	q
0	30–0.5*i*	0	30–0.5*i*
0.1	24.553–0.4092*i*	0.0278–0.0005*i*	24.538–0.4090*i*
0.2	20.022–0.3337*i*	0.0934–0.0016*i*	19.972–0.3329*i*
0.3	16.186–0.2698*i*	0.1791–0.0030*i*	16.090–0.2682*i*
0.4	12.875–0.2146*i*	0.2736–0.0046*i*	12.728–0.2121*i*
0.5	9.9502–0.1658*i*	0.3664–0.0061*i*	9.7539–0.1626*i*
0.6	7.2787–0.1213*i*	0.4419–0.0074*i*	7.0419–0.1174*i*
0.7	4.6802–0.0780*i*	0.4669–0.0078*i*	4.4301–0.0738*i*

Fig. 1

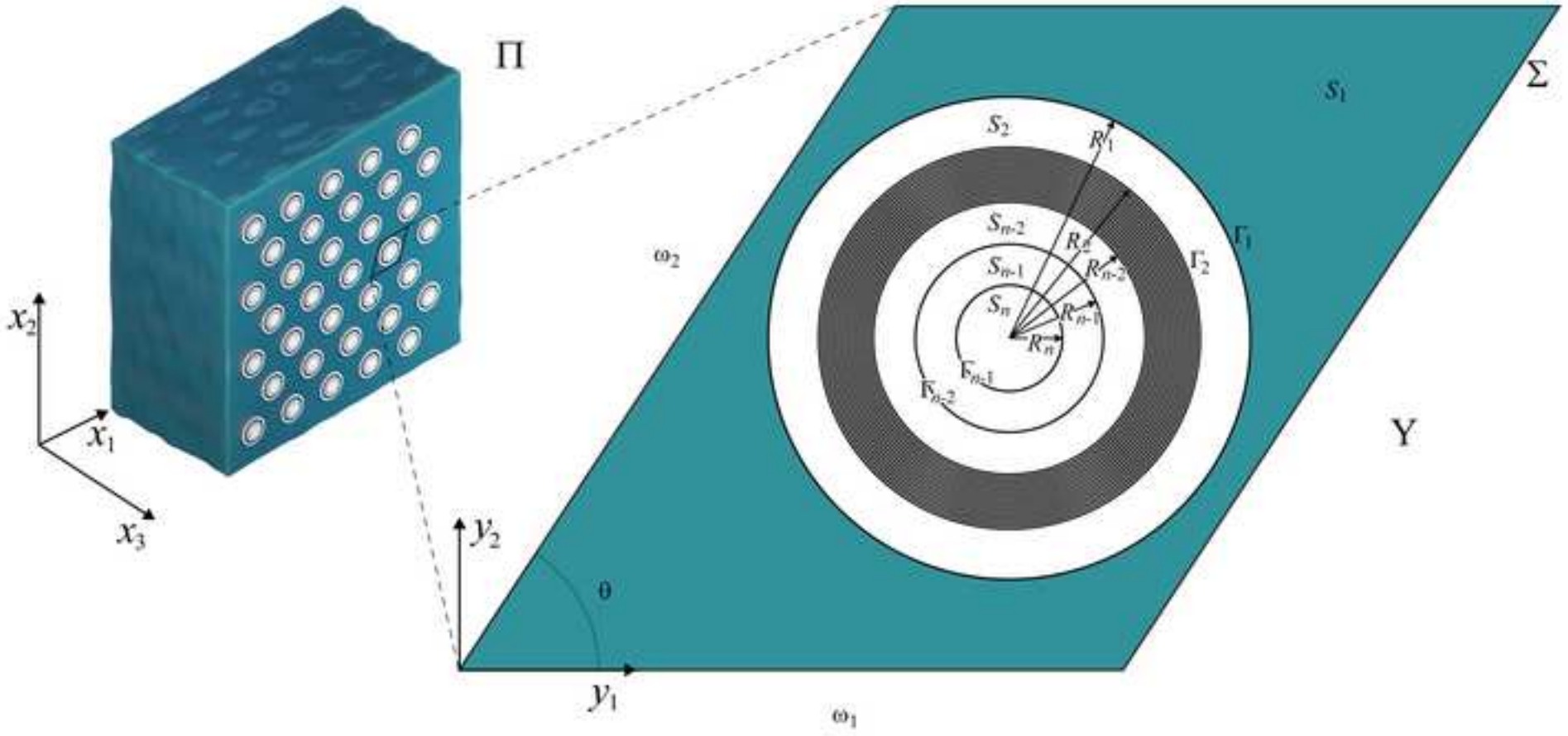
Π
Σ
s_1
S_2
R_1
S_{n-2}
R_2
S_{n-1}
R_{n-2}
S_n
R_{n-1}
R_n
Γ_1
Γ_2
Γ_{n-1}
Γ_{n-2}
ω_2
ω_1
Y
x_2
x_1
x_3
y_2
y_1
θ

Fig. 2

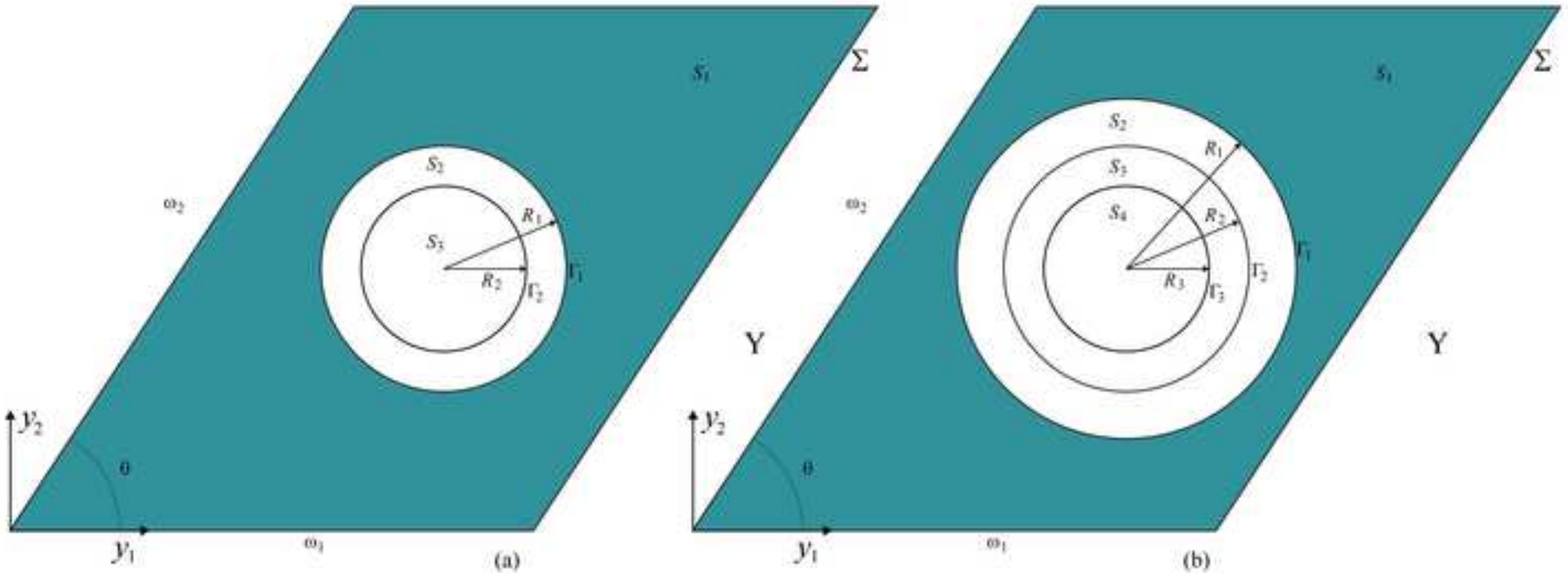
S_1
Σ
S_2
ω_2
R_1
S_3
R_2
Γ_1
Γ_2
y_2
θ
y_1
ω_1
(a)
S_1
Σ
S_2
R_1
S_3
ω_2
S_4
R_2
Γ_1
R_3
Γ_3
Γ_2
Y
Y
y_2
θ
y_1
ω_1
(b)

Fig. 3

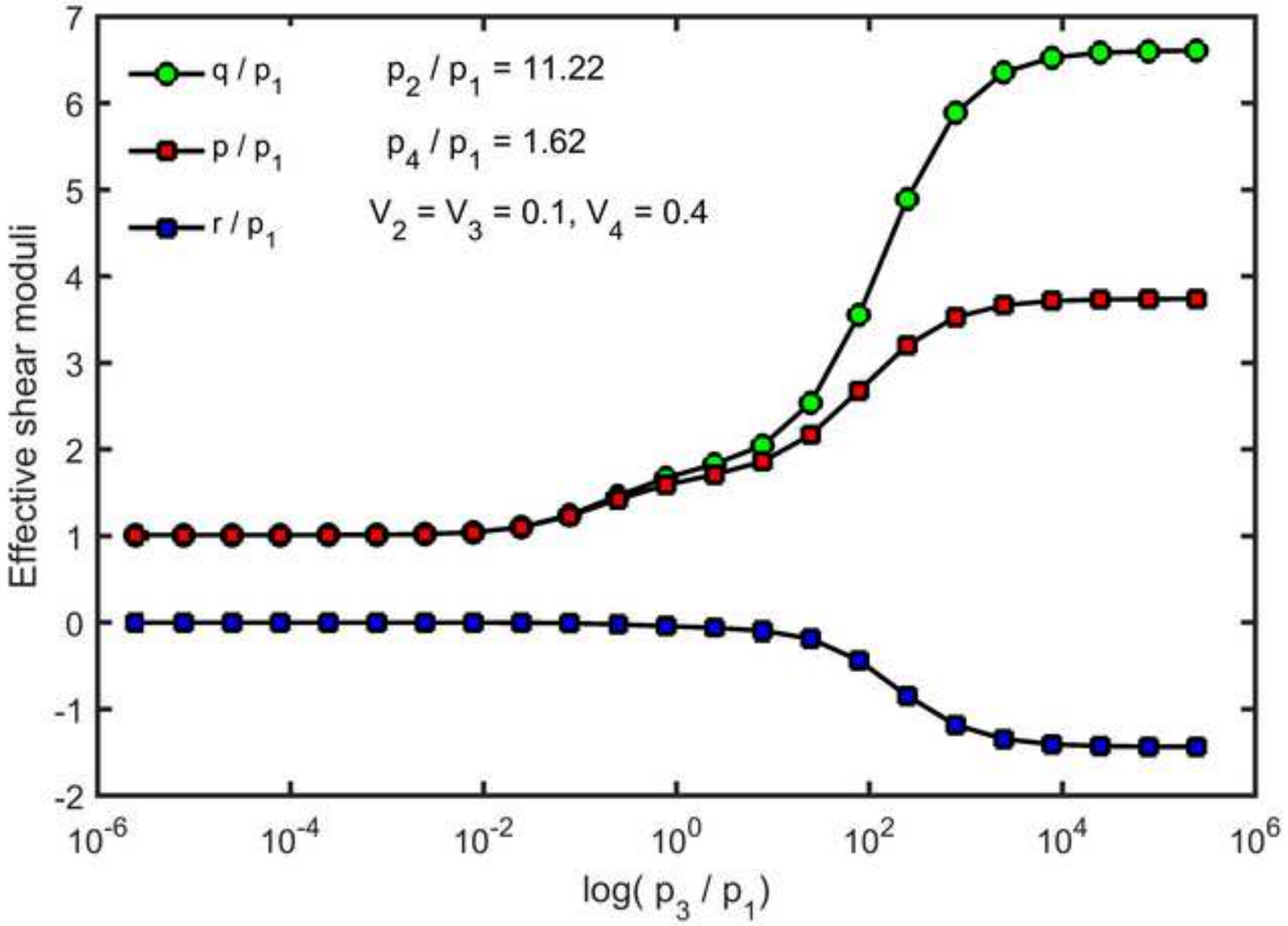
q / p1
p / p1
r / p1
p2 / p1 = 11.22
p4 / p1 = 1.62
V2 = V3 = 0.1, V4 = 0.4
Effective shear moduli
log(p3 / p1)
7
6
5
4
3
2
1
0
-1
-2
10-6
10-4
10-2
100
102
104
106

Fig. 4

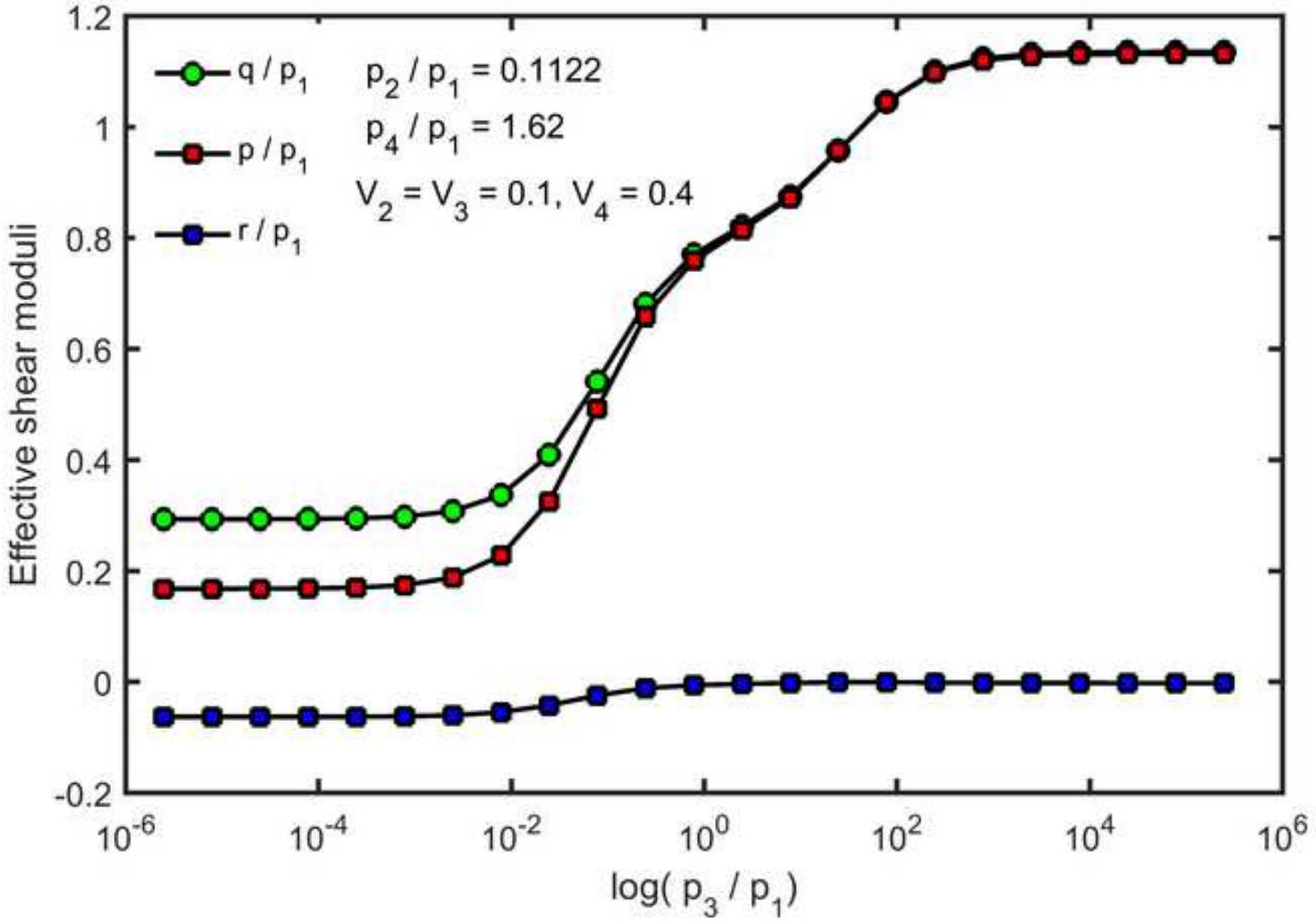
q / p1
p / p1
r / p1
p2 / p1 = 0.1122
p4 / p1 = 1.62
V2 = V3 = 0.1, V4 = 0.4
Effective shear moduli
log(p3 / p1)
1.2
1
0.8
0.6
0.4
0.2
0
-0.2
10-6
10-4
10-2
100
102
104
106

Fig. 5

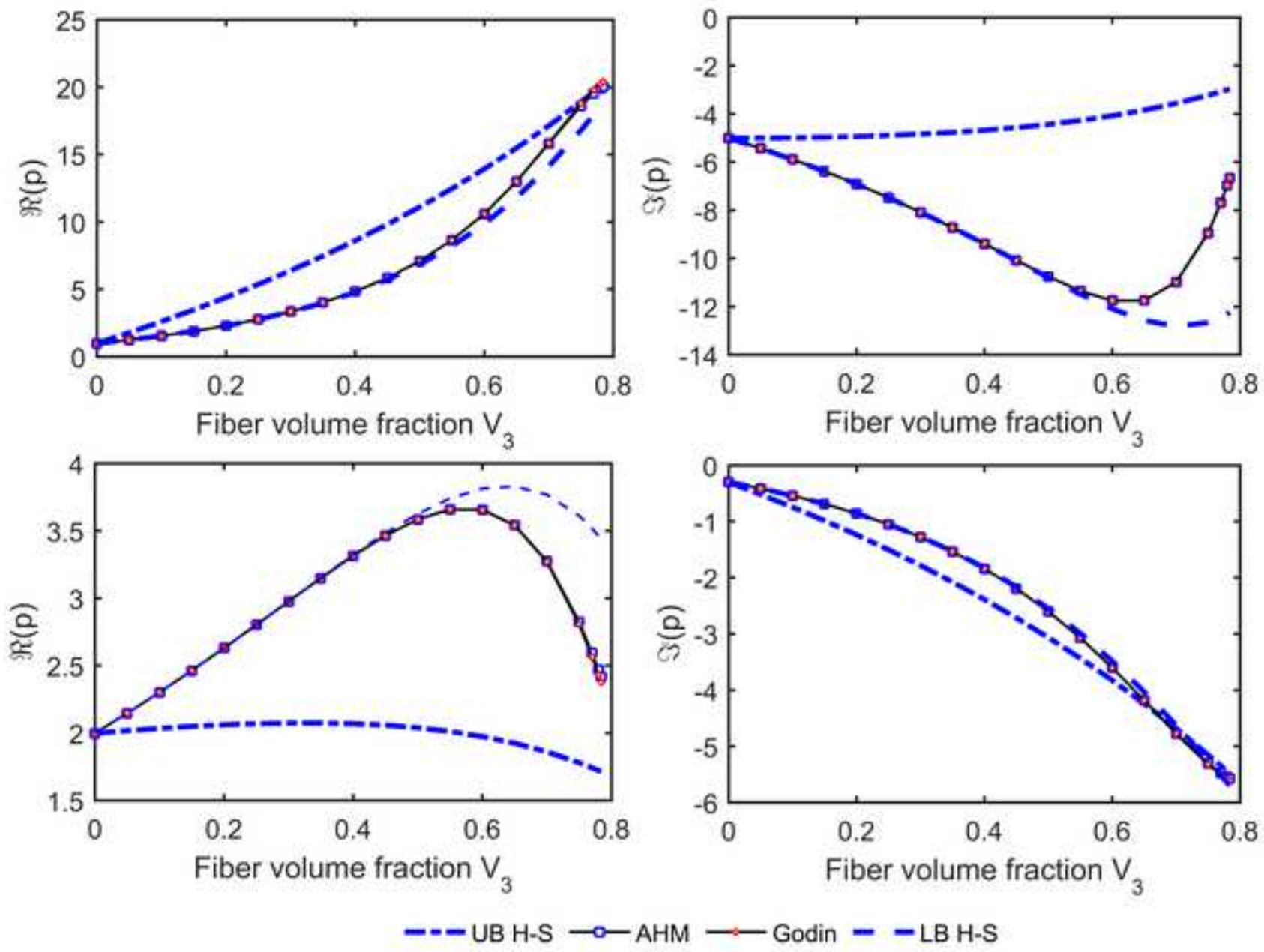
ℜ(p)
Fiber volume fraction V3
ℑ(p)
Fiber volume fraction V3
ℜ(p)
Fiber volume fraction V3
ℑ(p)
Fiber volume fraction V3
UB H-S
AHM
Godin
LB H-S

Fig. 6

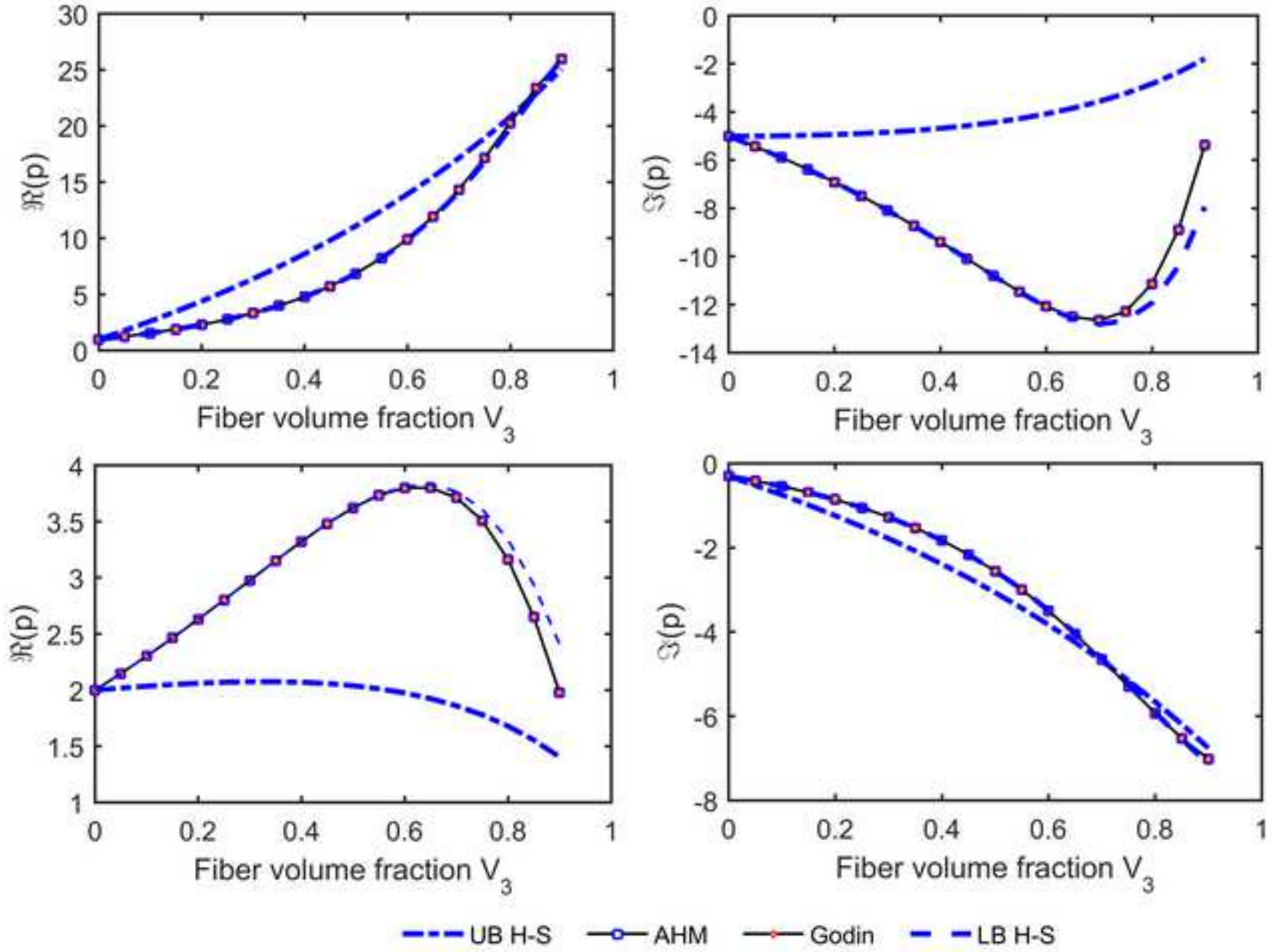
ℜ(p)
Fiber volume fraction V3
ℑ(p)
Fiber volume fraction V3
ℜ(p)
Fiber volume fraction V3
ℑ(p)
Fiber volume fraction V3
UB H-S
AHM
Godin
LB H-S

Fig. 7

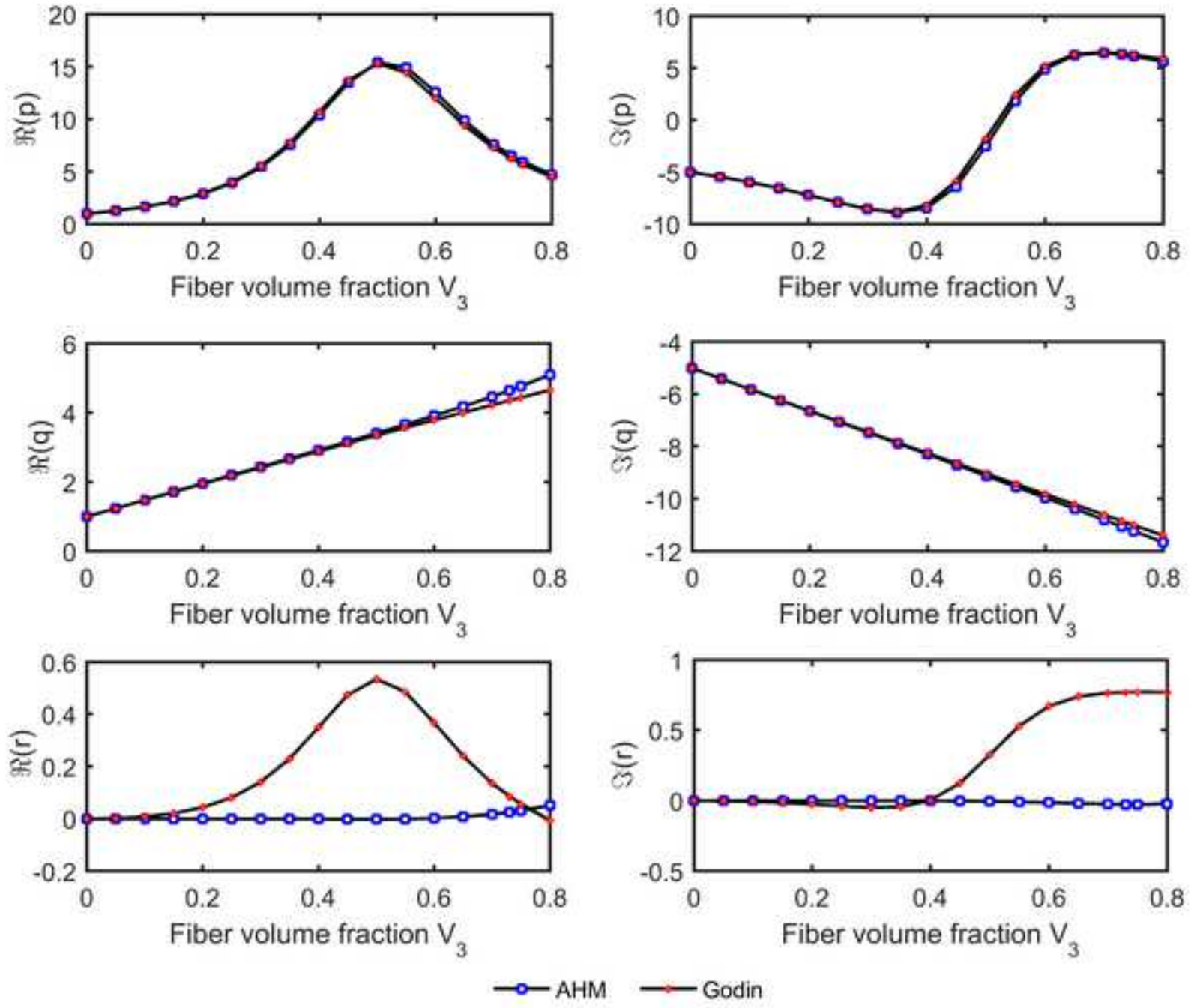

Fig. 8

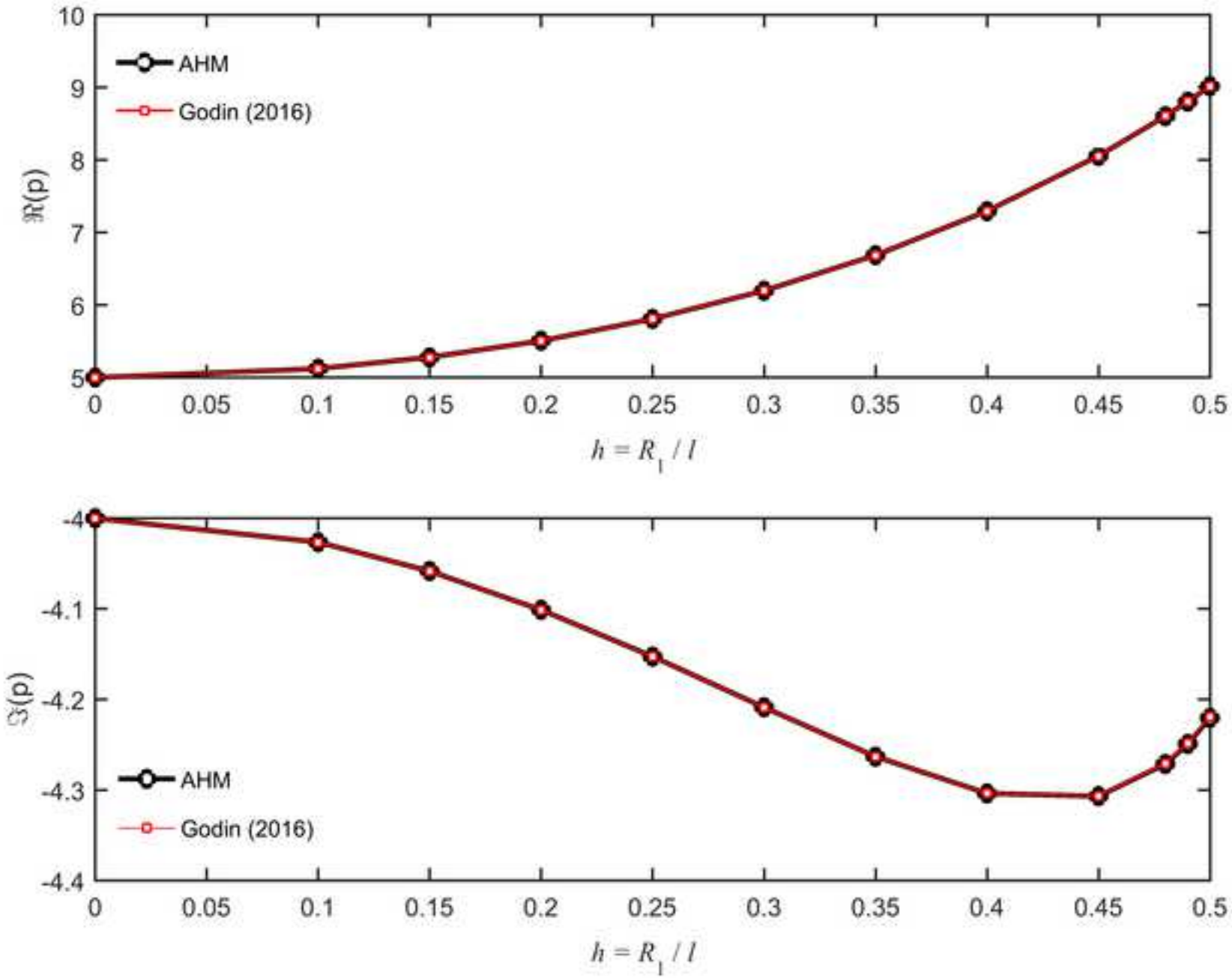
AHM
Godin (2016)
ℜ(p)
10
9
8
7
6
5
0
0.05
0.1
0.15
0.2
0.25
0.3
0.35
0.4
0.45
0.5
h = R1 / l
AHM
Godin (2016)
ℑ(p)
-4
-4.1
-4.2
-4.3
-4.4
0
0.05
0.1
0.15
0.2
0.25
0.3
0.35
0.4
0.45
0.5
h = R1 / l

Fig. 9

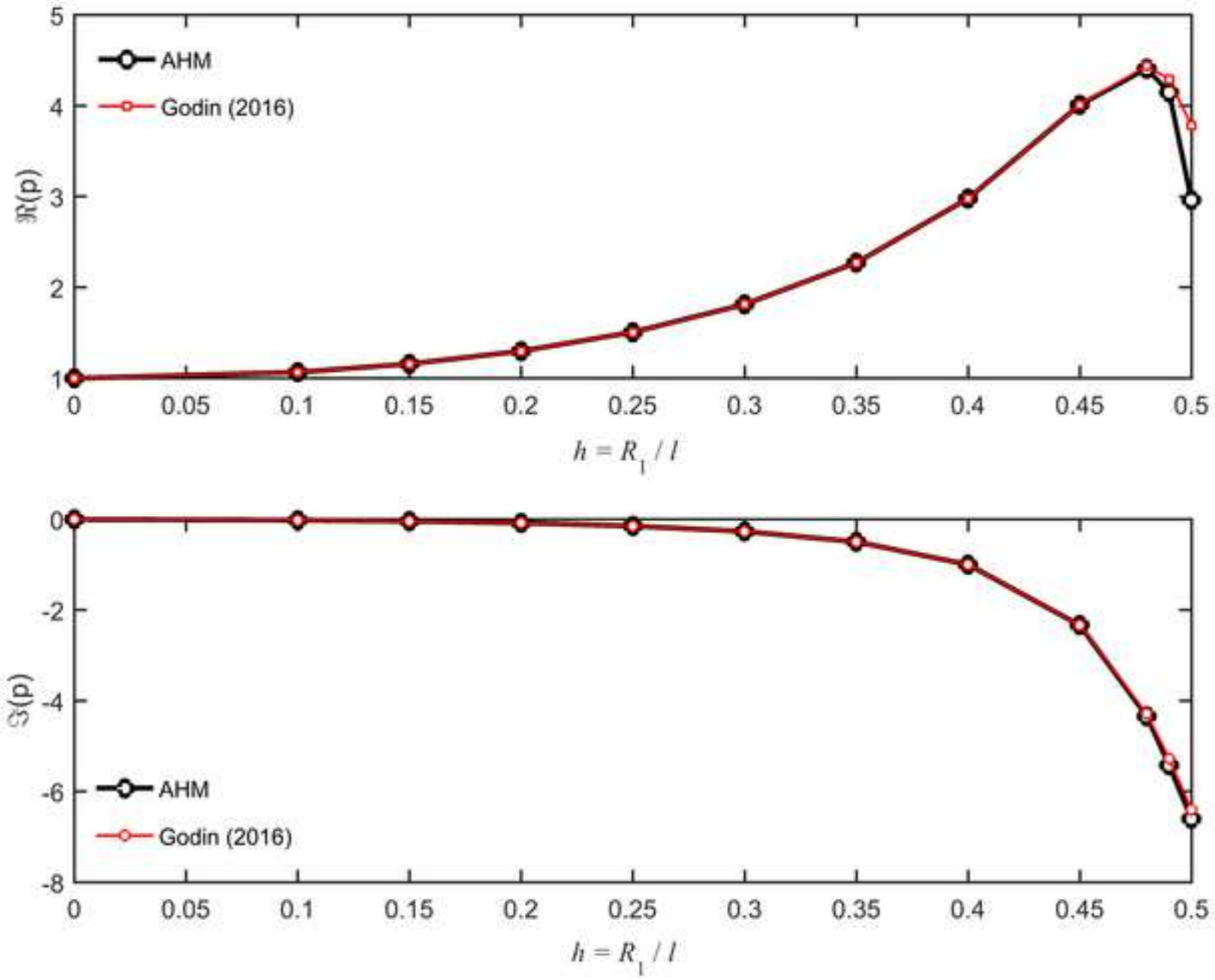

Fig. 10

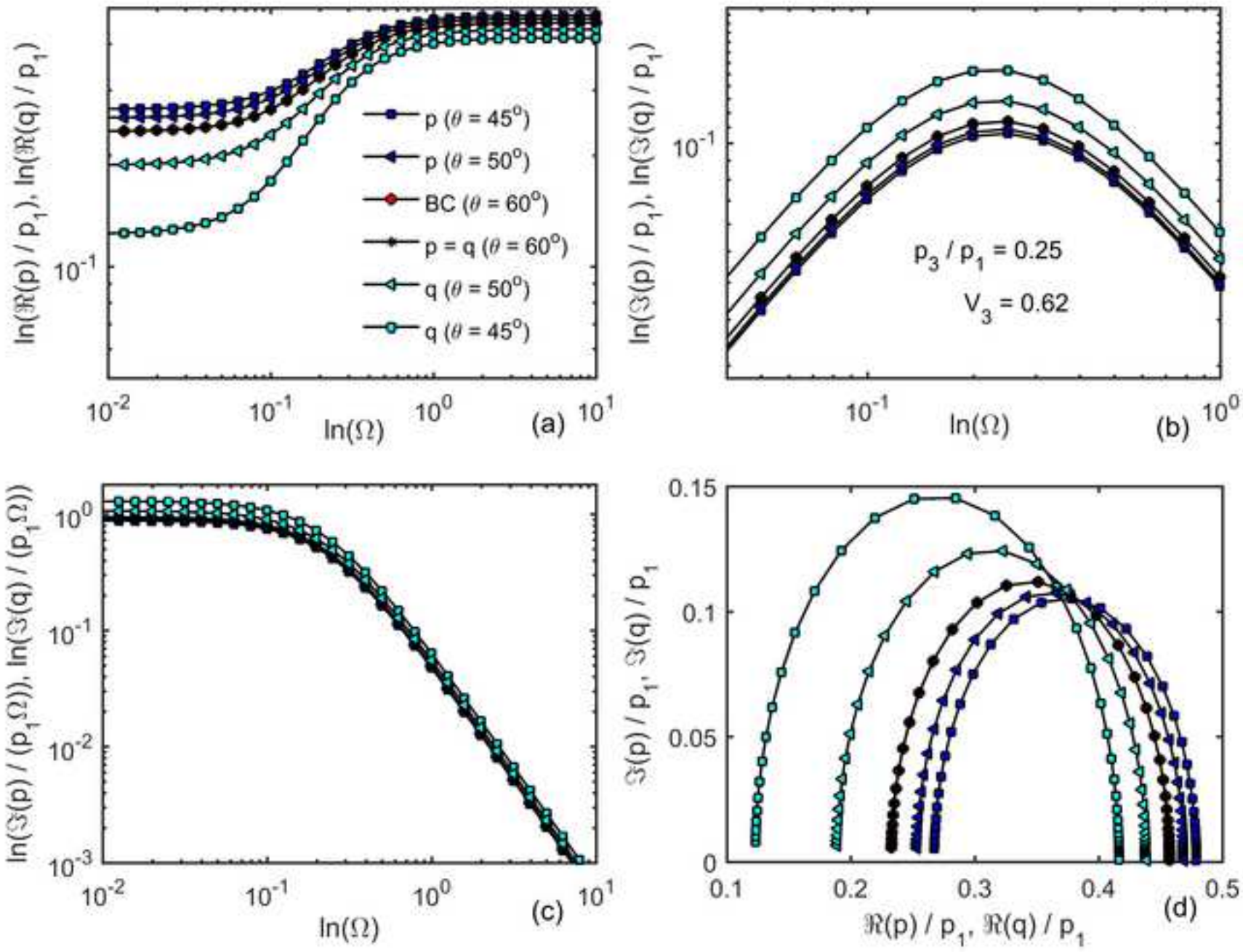
ln(ℜ(p) / p1), ln(ℜ(q) / p1)
p (θ = 45°)
p (θ = 50°)
BC (θ = 60°)
p = q (θ = 60°)
q (θ = 50°)
q (θ = 45°)
10-1
10-2
10-1
ln(Ω)
10^0
10^1
(a)
ln(ℑ(p) / p1), ln(ℑ(q) / p1)
p3 / p1 = 0.25
V3 = 0.62
10-1
ln(Ω)
10^0
(b)
ln(ℑ(p) / (p1Ω)), ln(ℑ(q) / (p1Ω))
10^0
10-1
10-2
10-3
10-2
10-1
ln(Ω)
10^0
10^1
(c)
ℑ(p) / p1, ℑ(q) / p1
0.15
0.1
0.05
0
0.1
0.2
0.3
0.4
0.5
ℜ(p) / p1, ℜ(q) / p1
(d)

Fig. 11

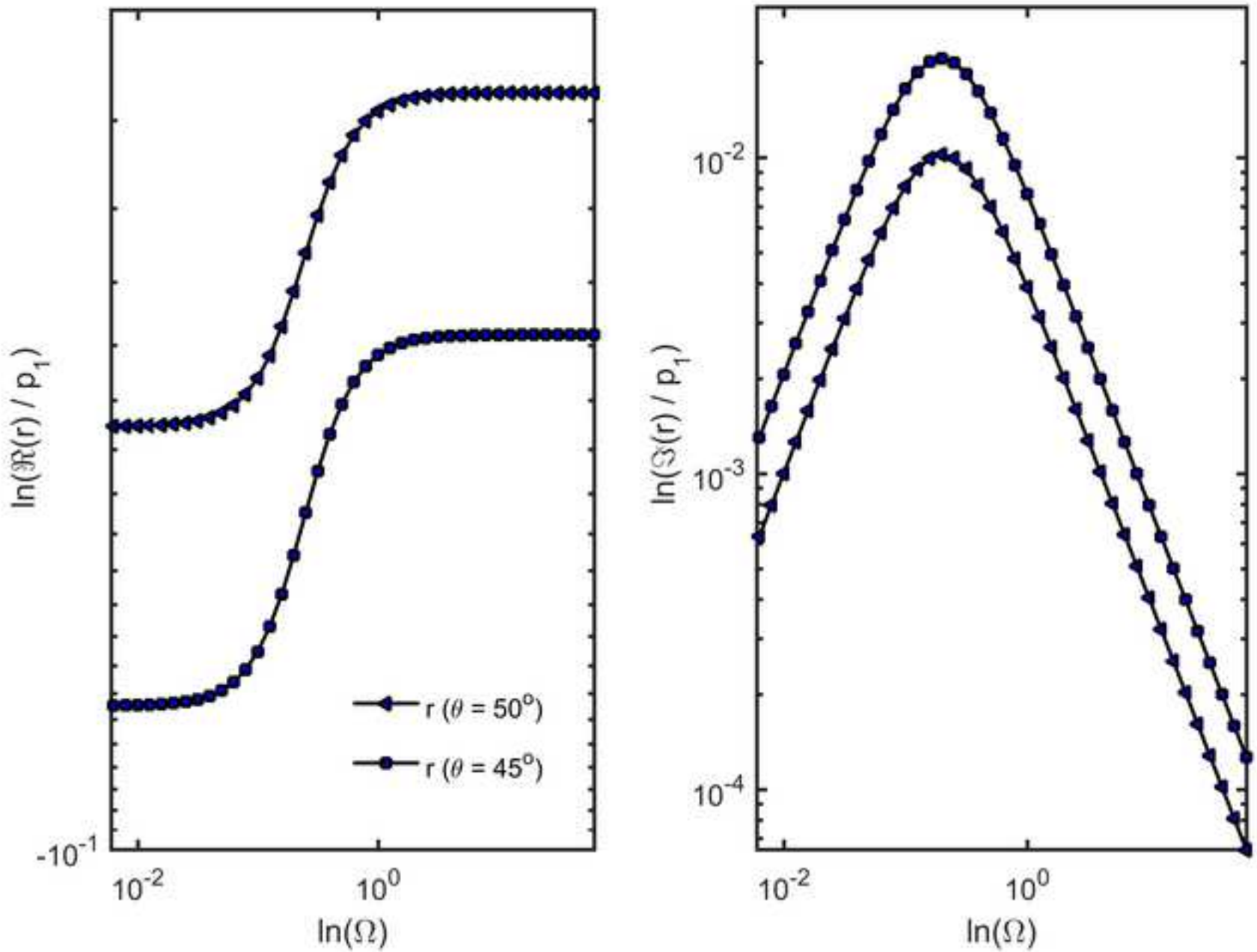
ln(ℜ(r) / p1)
-10-1
10-2
100
ln(Ω)
r (θ = 50°)
r (θ = 45°)
ln(ℑ(r) / p1)
10-2
10-3
10-4
10-2
100
ln(Ω)

Fig. 12

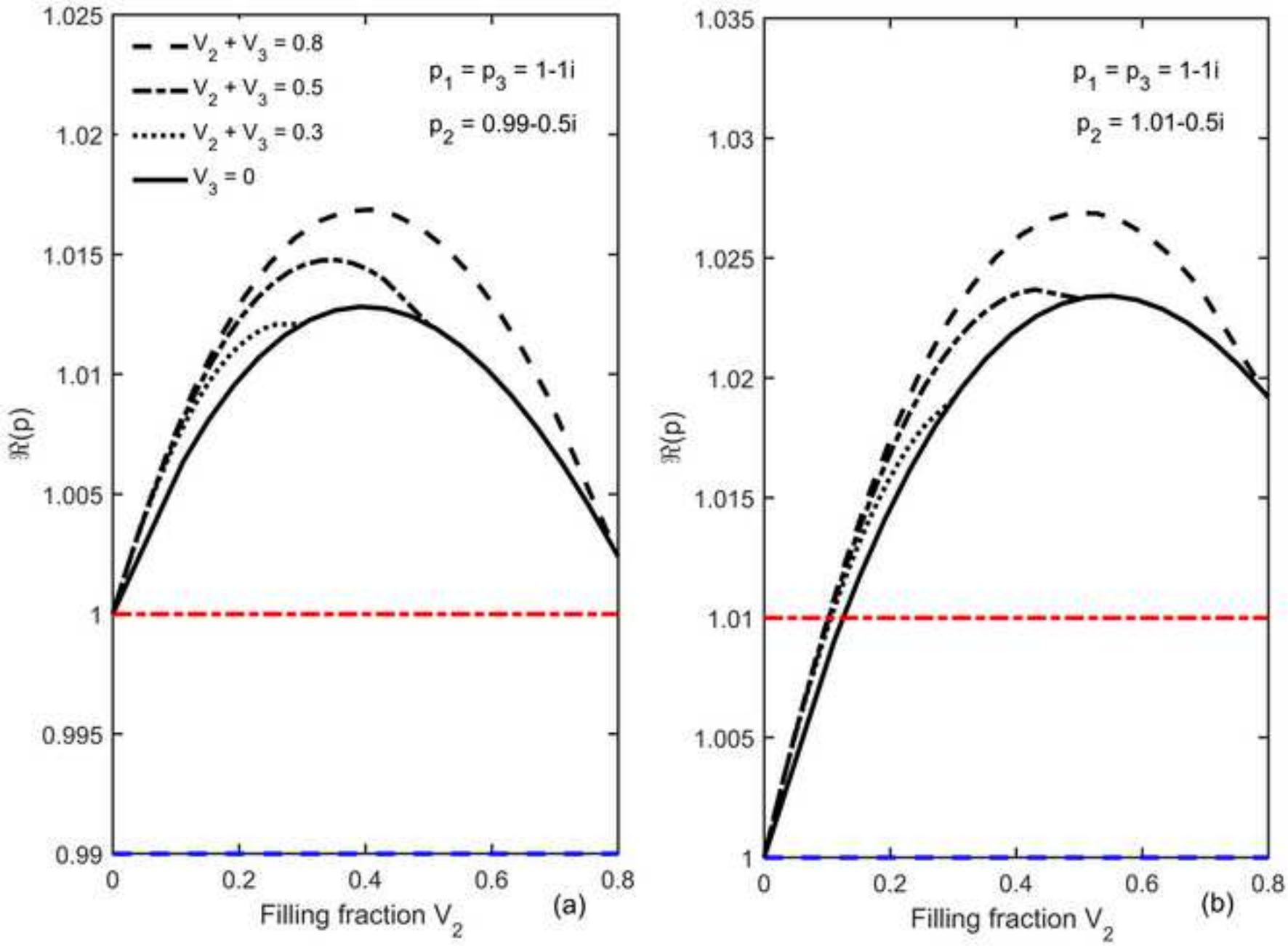
1.025
1.02
1.015
1.01
1.005
1
0.995
0.99
ℜ(p)
V2 + V3 = 0.8
V2 + V3 = 0.5
V2 + V3 = 0.3
V3 = 0
p1 = p3 = 1-1i
p2 = 0.99-0.5i
0
0.2
0.4
0.6
0.8
Filling fraction V2
(a)
1.035
1.03
1.025
1.02
1.015
1.01
1.005
1
ℜ(p)
p1 = p3 = 1-1i
p2 = 1.01-0.5i
0
0.2
0.4
0.6
0.8
Filling fraction V2
(b)